Title

Total Reconstitution of Receptor-mediated Ras Activation by SOS In Vitro

Author

Alvarez Rivera, Steven Alexis

Publication Date

2020

Peer reviewed|Thesis/dissertation

Total Reconstitution of Receptor-mediated Ras Activation by SOS In Vitro

By

Steven Alexis Alvarez Rivera

A dissertation submitted in partial satisfaction of the

requirements for the degree of

Doctor of Philosophy

in

Engineering – Materials Science and Engineering

in the

Graduate Division

of the

University of California, Berkeley

Committee in charge:

Professor Jay T. Groves, Co-Chair
Professor Kevin E. Healy, Co-Chair
Professor Phillip B. Messersmith
Professor Ke Xu

Spring 2020

Total Reconstitution of Receptor-mediated Ras Activation by SOS In Vitro

Abstract

Total Reconstitution of Receptor-mediated Ras Activation by SOS In Vitro

by

Steven Alexis Alvarez Rivera

Doctor of Philosophy in Materials Science and Engineering

University of California, Berkeley

Professor Jay T. Groves, Co-Chair

Professor Kevin E. Healy, Co-Chair

Ras GTPase activation is part of an important class of signaling reactions that take place on membrane surfaces in cells. This membrane-anchored protein functions as binary switch that relays information to many essential intracellular signaling pathways. Some of the most aggressive cancers are caused by mutations in Ras, making it a clinical target of paramount importance. Cells have evolved multiple layers of regulation that tightly control Ras signaling, including enzymes that control the activation state of Ras, membrane specificity, allosteric mechanisms, and two-dimensional protein phase transitions. At the center of this regulation is the guanine nucleotide exchange factor (GEF), Son of Sevenless (SOS). SOS is a key Ras activator that is autoinhibited in the cytosol and activates upon membrane recruitment in response extracellular stimuli. In addition to its GEF activity, SOS facilitates a phosphotyrosine-driven phase transition by crosslinking proteins at the membrane.

This dissertation aims to delve into the molecular processes and mechanisms behind the multilayered regulation of Ras activation by SOS. First, we extended an *in vitro* reconstitution platform of Ras on supported lipid bilayers (SLB) to include a real-time imaging readout of Ras activation. We engineered the Ras binding domain (RBD) of Raf1 kinase, which exhibits a natural selectivity for the active Ras-GTP state, to have rapid and fully reversible binding to Ras-GTP. This platform was then applied to the investigation of the allosteric activation of SOS and positive feedback. We found that allosteric Ras binding is a necessary, but not exclusive feature of a processive activation state observed in SOS. However, the nucleotide specificity in allosteric Ras binding promoted SOS processive activity, suggesting an alternate pathway to establish positive feedback in Ras activation. Finally, the Ras SLB platform was extended to include membrane inputs necessary to reconstitute the receptor-mediated recruitment of SOS and formation of two-dimensional protein assemblies. This work identified that the receptor-mediated membrane recruitment and release of autoinhibition introduces a kinetic threshold to the duration of SOS membrane dwells for effective signal propagation. The phosphotyrosine-driven phase transition modulates signaling by increasing the probability of SOS enzymes crossing this kinetic

threshold. Collectively, these findings are suggestive of a kinetic proofreading mechanism in Ras signaling, where spurious signals from short dwells are filtered, and true signals from long dwells are propagated and amplified by the processive activity of SOS.

To My Family

Contents

List of Figures

Acknowledgements

Conquering this milestone would have been impossible without the people that believed in me and supported me along the way. I would like to thank my mentors, colleagues, friends, and family for their support during my graduate school journey.

First, I would like to thank my research advisor, Prof. Jay T. Groves. I will always be indebted for the chance he took on me, a curious engineer with no background in biology or physical chemistry, in joining his group. I am grateful for his mentorship, patience, and for providing me the space to make mistakes and learn from them. He challenged me to think about the big picture, to be bold, and to go after the "big experiment", while giving me the scientific freedom to explore and pursue curiosity-driven questions. My years in the Groves Lab have been formative, shaping me into an independent and critical-thinking scientist. Thank you.

As a member of the Groves Lab, I have been blessed with the opportunity of interacting with and learning from some of the most talented scientists I have ever met. I want to thank Prof. Shalini Low-Nam for her mentorship, guidance, and friendship. Her unwavering belief in me, even when I had none, inspired me to embrace every challenge. I am grateful for her selflessness and investment in my growth as I scientist. She led by example and always set the highest standard for conducting science, pushing me to think critically and always exceed expectations. Among the most cherished memories I hold are our scientific discussions and brainstorming sessions in the Groves Lab. I want to thank Prof. Scott Hansen for his mentorship in my earliest days as a graduate student and for his friendship. I am thankful for his infinite patience and willingness to answer the "100 daily questions" of a freshly-minted graduate student with a severe case of imposter syndrome. He shared his technical know-how and taught me almost all the biochemistry and molecular cell biology skills I know today. His willingness to share ideas, reagents, and expertise gave me that initial push I needed to embark on a successful trajectory in the lab. I want to thank Dr. Jenny Lin, Dr. Monatrice Lam, Dr. William Huang, Prof. Jean Chung, Prof. Young Kwang Lee, and Emily Laubscher for the opportunity of working together on various projects throughout my years in the Groves lab. They have all contributed to the work presented in this dissertation and to my growth as a scientist. I remember fondly the many hours shared in the lab together and cherish our continued friendship.

I am grateful to all the members of the Groves Lab for creating a dynamic, vibrant, and collaborative environment to do science. In particular, I want to thank Dr. Sune Christensen, Dr. Hsiung Lin-Tu, Dr. Nicole Fay, Dr. Kate Alfieri, Dr. Michael Coyle, Dr. Meimei Dong, Dr.

Geoffrey O'Donoghue, Dr. Adrienne Green, Dr. Hiro Kai, Dr. Wan-Chen Lin, Dr. Hyuneil Kim, Dr. Darren McAffee, Cody Holik, Laura Nocka, Albert Lee, Joey DeGrandchamp, and Nugent Lew: they have all created strong and enduring impressions on me. I want to thank Laurie Mason for her administrative role in supporting my science, for all our chats, and for always looking out for me.

I want to thank Prof. John Kuriyan, Prof. Jeroen Roose, Prof. Valerie Weaver, Dr. Jesse Jun and Dr. Yasushi Kondo for fostering many fruitful collaborations that I was fortunate to be a part of.

I want to thank the Department of Materials Science and Engineering for giving me the opportunity to join their graduate program. In particular, I want to thank Prof. Oscar Dubon, Prof. Mark Asta, Catalina Estrada, and Ariana Castro for their wisdom and help in navigating graduate school.

My graduate career at UC Berkeley was only possible because of people that believed in me and supported my aspirations of a graduate career. I want to thank Dr. Alexander Hexemer and the team at beamline 7.3.3 at the Advanced Light Source (ALS) for giving me my first job opportunity after college and opening the doors for pursuing a graduate career. I want to thank Prof. Miguel Modestino for his advice and support in my transition from college to my job at the ALS and my move from Puerto Rico to the Bay Area. I want to thank Prof. Carlos Rinaldi, Prof. Madeline Torres-Lugo, and Prof. David Suleiman for their mentorship, advice, and support as an undergraduate student at UPR Mayaguez and for inspiring me to pursue a graduate career.

I am thankful for my friends outside lab for their constant encouragement: Dr. Jorge Santiago, Jessica Jimenez, Hector Martinez, Diana Rodriguez, Amneris Miranda, Prof. Geoffrey Graff, Dr. Willie Mae Reese, and Domingos Ng. Their friendship kept me grounded.

I thank my parents, Esteban Alvarez and Raquel Rivera, for all the sacrifices they made so I could be where I am today. The moral compass and strong work ethic they instilled in me from a young age continue to guide me to this day.

Last but not least, I want to thank Dr. Wes Wiltse for being my rock throughout this process. I thank him for always supporting my goals, even if it meant sleeping in lab while I ran experiments on the microscope at 3 in the morning. His unwavering support through this wild journey is what got me to the finish line.

Chapter 1

Introduction and background

1.1 Signal processing at the membrane

Cells are equipped with elaborate systems that can receive and process signals from their environment in order to make decisions. Signals are processed in the form of chemical modifications and circuits take the form of molecular assemblies that control the flow of information. A key aspect of signal transduction in cells is that signaling reactions originate at the cellular membrane(*1*). Membrane physicochemical properties give rise to many emergent properties in chemical reactions, including local concentration enhancement effects on intrinsic rates, polarization, and geometry sensing(*1*, *2*). It is therefore imperative to study signaling initiation in its native membrane environment.

An important class of chemical reactions that takes place on cell membrane surfaces is the activation of guanosine triphosphatases (GTPases) of the small G-protein family. GTPases are small globular membrane-anchored proteins that generally serve as binary molecular switches(*3*). They cycle between "ON" and "OFF" states and regulate a wide range of essential aspects to cell function, such as intracellular trafficking, cell shape and cytoskeleton rearrangement, migration, and proliferation(*4*).

Within the small G-protein superfamily, Ras GTPases stand out for their prominent role in cancer. Ras regulates a variety of important signaling pathways that result in cellular proliferation (e.g. to replace damaged tissue) and differentiation (e.g. cell type establishment). Mutations in genes that encode for Ras proteins often lead to hyperactivation of Ras signaling and drive more than 30% of all human cancers(*5*). Despite three decades of focused efforts and recent promising results(*6*–*9*), therapeutic targeting remains elusive. The picomolar affinity for nucleotide binding and its relatively smooth surface has made targeting of Ras extremely difficult(*5*). Therefore, developing new methods to further resolve mechanistic details of Ras function and regulation will be key in finding new features in Ras that can be exploited for therapeutic targeting.

1.2 Ras activation/deactivation cycle

Ras switch function originates from the binding of guanosine nucleotides with high affinity and hydrolyzing guanosine triphosphate (GTP) to guanosine diphosphate (GDP) and

an inorganic phosphate(*3*) (Figure 1.1). Its activation state is determined by the identity of the guanosine nucleotide bound to Ras: GDP-bound Ras is inert, while GTP binding induces a conformational change that promotes effector binding and signal propagation. Signal termination is controlled by the irreversible hydrolysis of GTP.

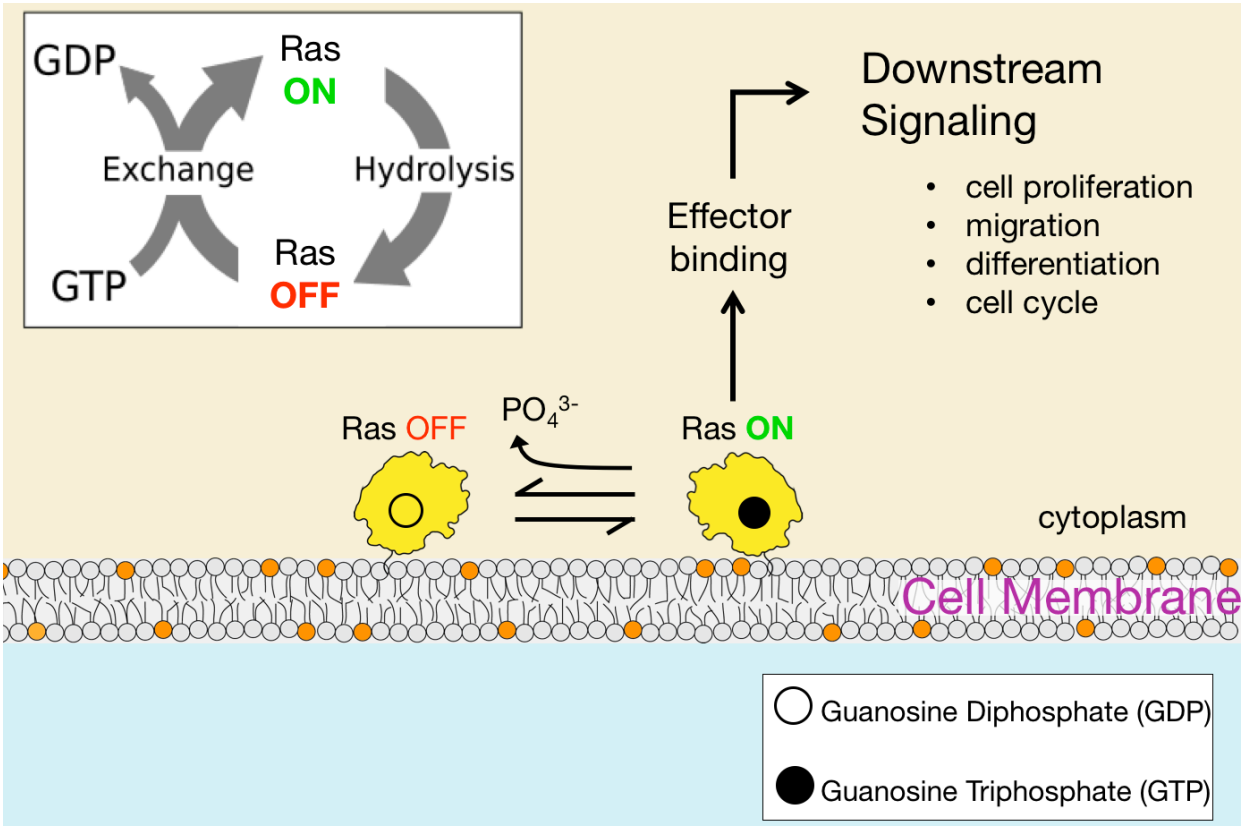

Fig. 1.1| Ras activation cycle. Ras GTPases function as binary switches. The activation state is determined by the guanosine nucleotide bound to Ras, where GTP-bound Ras is active and GDP-bound Ras is inactive. The switch cycles "ON" by exchanging GDP-bound Ras to GTP and "OFF" by hydrolyzing GTP to GDP and a free phosphate.

"ON" / "OFF" cycling is tightly controlled by regulatory enzymes that are coupled to other cellular signals(*10*). Activation of Ras is mediated by guanosine exchange factors (GEFs) that facilitate GDP dissociation from Ras. Activators are recruited to the membrane in response to extracellular cues. When localized to the membrane, the activator binds to Ras, lowers its affinity for the bound nucleotide, and promotes nucleotide release. This allows GTP, which is present in excess in the bulk solution, to bind and activate Ras. Deactivation is catalyzed by GTPase activating proteins (GAPs) that bind to Ras and accelerate GTP hydrolysis.

1.3 Multilayered regulation and membrane-dependent signal integration by the activator SOS

Cells have evolved multiple layers of regulation that tightly control Ras signaling. This is exemplified by the layered regulation observed in the Ras GEF Son of Sevenless (SOS). SOS is a ubiquitously expressed Ras GEF(*11*) and a key gatekeeper of Ras activation. It has a multi-domain structure that enables modular control of its enzymatic activity (Figure 1.2B). SOS is comprised of a catalytic core that has a Ras exchanger motif (REM) and a Cdc25 domain, flanked by a proline rich (PR) C- terminal domain and histone-fold (HF), plecksterin homology (PH), and Dbl homology (DH) N- terminal domains(*12*). These domains contribute positive feedback, allosteric regulation, autoinhibition, and lipid binding features in SOS, regulating its activity in the context of membrane surfaces(*12*).

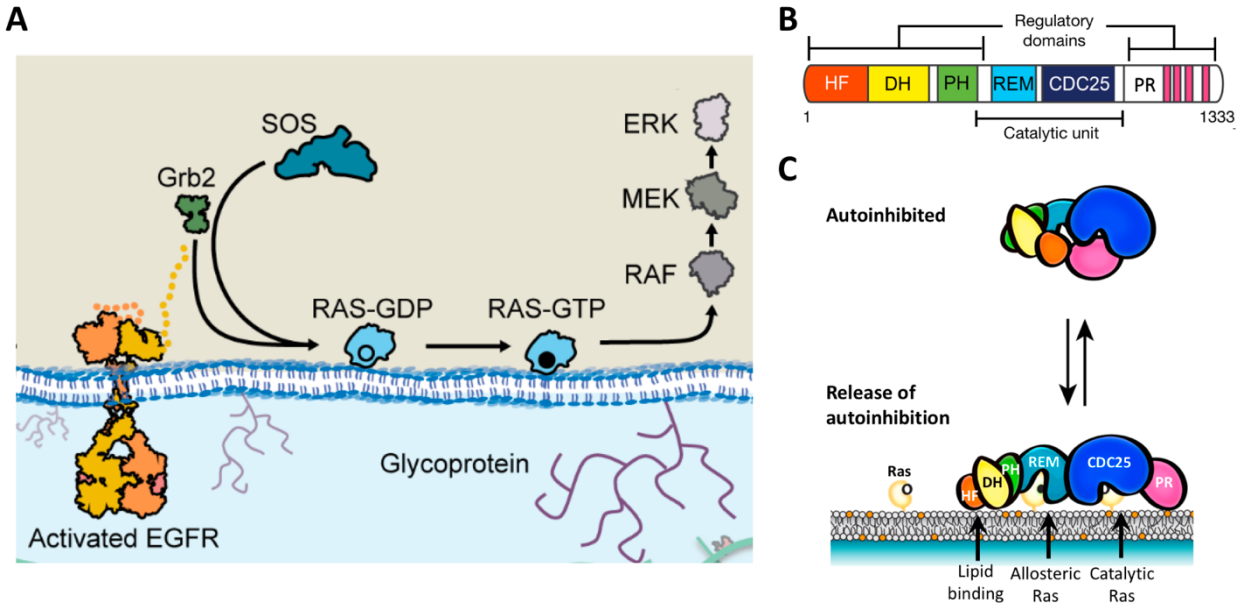

Fig. 1.2| The activation of Son of Sevenless (SOS). A, Schematic of receptor-mediated SOS activation. Activated receptors recruit SOS to the membrane surface via the adaptor protein Grb2. Interactions with membrane lipids induce the release of autoinhibition in SOS and promote nucleotide exchange activity on substrate Ras. **B,** Domain organization of SOS. SOS is comprised of a catalytic core flanked with N- and C-terminal regulatory domains. **C,** Schematic of release of autoinhibition in SOS upon membrane recruitment. N- and C- flanking domains contribute to an autoinhibited conformation in solution. Lipid interactions of the plecksterin homology (PH) and histone-fold (HF) domains release autoinhibition and enable Ras binding to allosteric and catalytic sites.

Receptor-mediated Ras activation by SOS is a multistep process. The N- and C- terminal regulatory domains contribute to an autoinhibited conformation of the enzyme(*13–15*), believed to be the predominant state of SOS in the cytosol (Figure 1.2C). SOS activation is initiated by the activation of cell surface receptors, such as the T-Cell receptor (TCR) and epidermal growth factor receptor (EGFR), that induce the translocation of SOS to the plasma

membrane, where substrate Ras is present (Figure 1.2A). Recruitment of SOS to the membrane is mediated by the adaptor protein Grb2, which simultaneously binds the PR motifs in the C- terminus of SOS and phosphorylated tyrosines of membrane receptors or transmembrane adaptor proteins(*16*–*21*). Once in the proximity of the membrane, the HF and PH domains in the N- terminus of SOS are believed to interact with anionic lipids, such as phosphatidylinositol 4,5-bisphosphate (PIP2) and phosphatidic acid (PA) lipids, promoting the release of SOS autoinhibition(*22*, *23*) (Figure 1.2C). As a result, a distal allosteric Ras binding site interposed between the Cdc25 and REM domains is exposed and able to bind active Ras, a necessary step for SOS activation(*13*, *22*–*25*). Allosteric Ras binding induces a structural change in the Cdc25 domain, that enables binding of Ras in the active site and catalysis of nucleotide exchange. Altogether, the multiple interactions of the N- and C- terminus of SOS at the membrane surface and allosteric Ras binding are predicted to act in concert to relieve autoinhibition and activate SOS, resulting in downstream Ras signal propagation(*25*, *26*).

1.4 Allosteric activation of SOS on lipid membranes

The allosteric binding of Ras-GTP to SOS confers this GEF unique sensitivity to the membrane surface context of the reaction and has profound implications in Ras signaling (*1*). *In vitro* measurements have shown that SOS-catalyzed nucleotide exchange rate increases by 500-fold when substrate Ras is presented on membranes versus in solution and is sensitive to the density of Ras-GTP on the membrane(*22*). This allosteric pocket in SOS has a 10-fold higher affinity for GTP-bound Ras (Ras-GTP) over GDP-bound Ras (Ras-GDP)(*13*), resulting in a positive feedback loop that has been implicated in switch-like cellular responses of receptor-induced Ras signaling(*27*).

Allosteric Ras binding to SOS introduces another important implication to Ras signaling: the potential for anchoring SOS to membranes. Reconstitution experiments on Ras-decorated supported lipid bilayers (SLBs) have shown that SOS truncations lacking the Grb2 binding domain or lipid binding domains can be recruited to membranes through Ras(*15*, *22*, *28*, *29*). In agreement with this observation, SOS constructs lacking the Grb2-binding domain localize to membranes in response to receptor-triggering and remain fully signaling competent(*25*, *30*–*33*). Single SOS molecules can dwell on membranes for extended periods, up to minutes, and processively activate thousands of substrate Ras in a single residency period(*28*, *29*). Furthermore, the single-molecule kinetic traces showed that SOS samples a broad spectrum of turnover rates by stochastically fluctuating between long-lived functional states, including highly active processive states(*28*). These highly processive states have been observed in a range of SOS constructs *in vitro*, from the minimal catalytic core to the full-length protein(*15*, *28*), suggesting it is a bona fide feature of this GEF and potentially a functional state of SOS in the cellular context.

1.5 SOS-mediated molecular assemblies

An emerging feature in cellular systems is the ability of biomolecules to form phase separated condensates (*34*, *35*). In addition to its GEF activity, SOS has been shown to mediate the formation of protein assemblies (*36*, *37*). In the context of T-Cells, multivalent interactions between the Grb2, SOS, and the membrane scaffold protein linker for activation of T-Cells (LAT) enables the formation of a networked assembly of LAT-Grb2-SOS on the membrane surface (Figure 1.3). The role of this protein assembly in regulating MAPK signal propagation remains an area of open investigation.

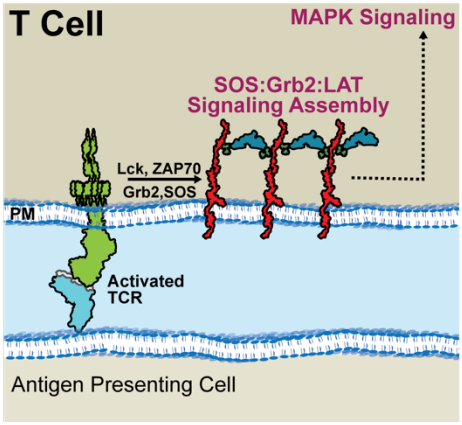

Fig. 1.3| SOS-Grb2-LAT molecular assembly. Schematic of receptor-mediated activation of SOS in T-Cells. T-Cell receptor triggering results in the activation of kinases that phosphorylate tyrosines (pY) in LAT. Multivalency of the pY sites on LAT, which serve as binding sites for Grb2, enables the networked assembly of LAT-Grb2-SOS into a condensed two-dimensional gel or liquid phase on the membrane surface.

1.6 Research Focus

A key aspect of Ras biology is that reactions occur in a membrane environment. The role of the membrane in regulating Ras signaling has only been partially investigated due to the inaccessibility of membranes to classic methods of study. This dissertation aims to expand the *in vitro* reconstitution approaches for the interrogation Ras signaling on membranes. Chapter 2 describes the extension of a Ras-supported lipid bilayer platform by introducing a real-time imaging readout of Ras activation on membranes. Chapter 3 shows the implementation of the Ras-SLB platform to dissect molecular features of the allosteric activation of SOS and positive feedback. Finally, Chapter 4 describes the total receptor-mediated reconstitution of SOS activation on supported membranes, where the role of 2-dimensional protein assembly in modulating signaling is investigated.

Chapter 2

Engineering a fast, selective, label-free, and fully reversible imaging-readout of Ras activation state on supported membranes

2.1 Abstract

Ras is a membrane-anchored protein that serves as a hub in many essential intracellular signaling pathways and it is often mutated in cancer. Ras switches between guanosine triphosphate (GTP)-loaded active (Ras-GTP) and guanosine diphosphate (GDP)-loaded inactive (Ras-GDP) states, and extensive cellular signaling activity and regulation is focused on controlling the activation state of Ras. Although various methods to assay Ras activity exist, this remains a difficult and largely unmet need, especially in the context of the membrane environment. Here, we engineered the Ras binding domain (RBD) of Raf1 kinase, which exhibits a natural selectivity for the active Ras-GTP state, to have rapid and fully reversible binding to Ras-GTP. Notably, an underappreciated native dimerization tendency of the wildtype RBD had to be removed. The engineered RBD sensor can be fluorescently labeled and used to monitor Ras activation state on membrane surfaces in imaging mode by TIRF microscopy. Finally, we demonstrate the utility of this assay in reporting enzyme catalyzed Ras activation, deactivation, and dynamic cycling in the context of a membrane. This approach is applicable to the characterization of competitive binding inhibitors targeting Ras mutants as well as molecules that modulate the activity of Ras or regulatory enzymes.

2.2 Introduction

Ras proteins function as binary molecular switches that alternate between “OFF” GDP-bound state (Ras-GDP) or “ON” GTP-bound state (Ras-GTP). Ras-GDP is inert, whereas GTP binding induces a conformational change that promotes effector binding and signal propagation(*3*). With more than ten distinct Ras effectors identified(*5*), Ras signaling is at the core of diverse intracellular processes, including gene expression, motility, cell-cycle progression, apoptosis, and survival(*4*).

CHAPTER 2. Engineering a fast, selective, label-free, and fully reversible imaging-readout of Ras activation state on supported membranes

The activation state of Ras is tightly controlled by regulatory enzymes that are activated in response to extracellular stimuli. Guanine nucleotide exchange factors (GEFs) activate Ras by catalyzing the exchange of GDP-bound Ras to GTP(*38*, *39*). GTPase activating proteins (GAPs) inactivate Ras by catalyzing the hydrolysis of GTP-bound Ras to GDP and inorganic phosphate(*40*, *41*). The existence of at least six families of Ras GAPs and three families of Ras GEFs further underscores the intricate fine-tuning in Ras signaling(*41*, *42*). Dysregulation of Ras signaling is a known contributor to human disease, with Ras genes being the most frequently mutated oncogenes in human cancer(*5*). Ras is a major target for cancer therapeutics; however, despite three decades of focused efforts and recent promising results(*6*–*9*), Ras inhibitors remain an unmet challenge.

A critical aspect of Ras biology that has been only partially investigated is the influence of its native membrane environment. The role of the plasma membrane in regulating Ras signaling is multifold. Translocation and membrane-mediated activation of regulatory and effector enzymes are central in Ras signal propagation(*43*–*45*). Ras orientation and spatial organization on membranes have also been implicated on regulating Ras signaling output(*46*). Furthermore, constraining reactions to 2-dimensional membrane surfaces can influence reaction intrinsic rates and dynamics(*1*), and can give rise to emerging properties, such as polarization and geometry sensing(*2*).

In vitro reconstitution of Ras proteins on supported membranes enables detailed interrogation of Ras function in a membrane environment. This method has already revealed novel membrane-specific regulatory mechanisms in Ras activation by the GEF Son of Sevenless (SOS). Discoveries using this platform include enhancement of SOS activity on membranes(*22*), SOS processive activity(*28*, *29*), C-terminal domain contributions to SOS inhibition(*15*), and kinetic proof reading in SOS activation(*47*). However, the study of Ras switch function in this assay is limited by the probes available to measure Ras activity. Nucleotides with fluorescent labels suitable for microscopy imaging techniques are typically used to monitor Ras activity on supported membranes. These probes have several disadvantages. First, they only report nucleotide exchange. Nucleotide hydrolysis, an essential part of Ras switch function, is not measurable in this assay. Second, these probes are single-turnover reporters. Once a Ras molecule exchanges its bound labeled nucleotide, it becomes invisible to the imaging assay. These limitations preclude the study of the dynamics of Ras switch cycling and the signaling output of GAP/GEF competition reactions, which have been suggested to play an important role in maintaining tonic Ras signaling(*42*). Finally, modified nucleotides can alter reaction kinetics(*48*) and can also be prohibitively expensive.

A different approach for detecting active Ras involves using the RBD domain of Raf1, which naturally binds Ras-GTP with high affinity. RBD is commonly used in pull down assays that measure the fraction of active Ras from cell lysates and in live cell imaging to detect spatiotemporal dynamics of Ras-GTP in cells. A less explored use of RBD is as a real-time

imaging readout of Ras activity *in vitro*. Coyle and colleagues(*49*) demonstrated this use of RBD in measuring the activation dynamics of Ras adsorbed on microspheres. However, reconstituting Ras by adsorption on solid surfaces potentially alters the output dynamics of this assay; lateral diffusion of Ras on membranes and signaling lipids needed to activate regulatory enzymes are expected to play a key role in feedback mechanisms and strongly influence Ras activation dynamics. In this work, we engineered the RBD of Raf1 kinase as a real-time, fully reversible, and fluorescence-based imaging readout of Ras activity on supported membranes. Characterizing the interaction between membrane-anchored Ras and RBD revealed that, while highly specific for Ras-GTP, RBD exhibits binding kinetics suggestive of dimers or oligomeric complexes at the membrane. This previously unknown property of RBD encumbers binding kinetics with complexation kinetics, complicating its use as a reporter for Ras activation state. Systematic examination of labeling strategies on RBD sensors shows that N- terminal tagging of RBD simplifies the sensor kinetics by disrupting RBD:Ras-GTP membrane oligomers. We characterized this sensor as a reporter of GEF-mediated Ras activation, GAP catalyzed Ras deactivation, and dynamic cycling of Ras in GAP/GEF competition reactions on supported membranes.

2.3 N-terminal tagging of RBD sensor exhibits clean 1st order kinetics

The experiment platform was expanded from a method for reconstituting Ras GTPases on supported lipid bilayers (SLBs)(*22*). SLBs consisting of 94% EGG-PC (L-α-phosphatidylcholine), 3% DOPS (1,2-dioleoyl-sn-glycero-3-phospho-L-serine), and 3% MCC-DOPE {1,2-dioleoyl-sn-glycero-3-phosphoethanolamine-N-[4-(p-maleimidomethyl) cyclohexane-carboxamide]} were deposited on glass substrates by vesicle fusion. H-Ras (from here on referred to as "Ras") was covalently attached to membranes via maleimide chemistry with the MCC-DOPE lipids. Membrane-coupled Ras retained lateral mobility and densities were measured to be ~2,000 μm^{-2}, comparable to the >1,000 μm^{-2} densities reported for Ras clusters in cells(*46*, *50*, *51*).

The strategy for measuring Ras activation involved monitoring RBD binding to membrane-coupled Ras (Fig. 2.1a). Ras-decorated SLBs were exposed to a solution of fluorescently labeled RBD. Because the binding reaction is constrained to the two-dimensional membrane surface, total internal reflection fluorescence (TIRF) microscopy – a surface-selective imaging technique – was used to monitor RBD binding to active Ras. The exponentially decaying illumination field from the surface in TIRF microscopy enables selective excitation and detection of RBD bound to membrane-coupled Ras, while non-bound molecules in solution remain undetected.

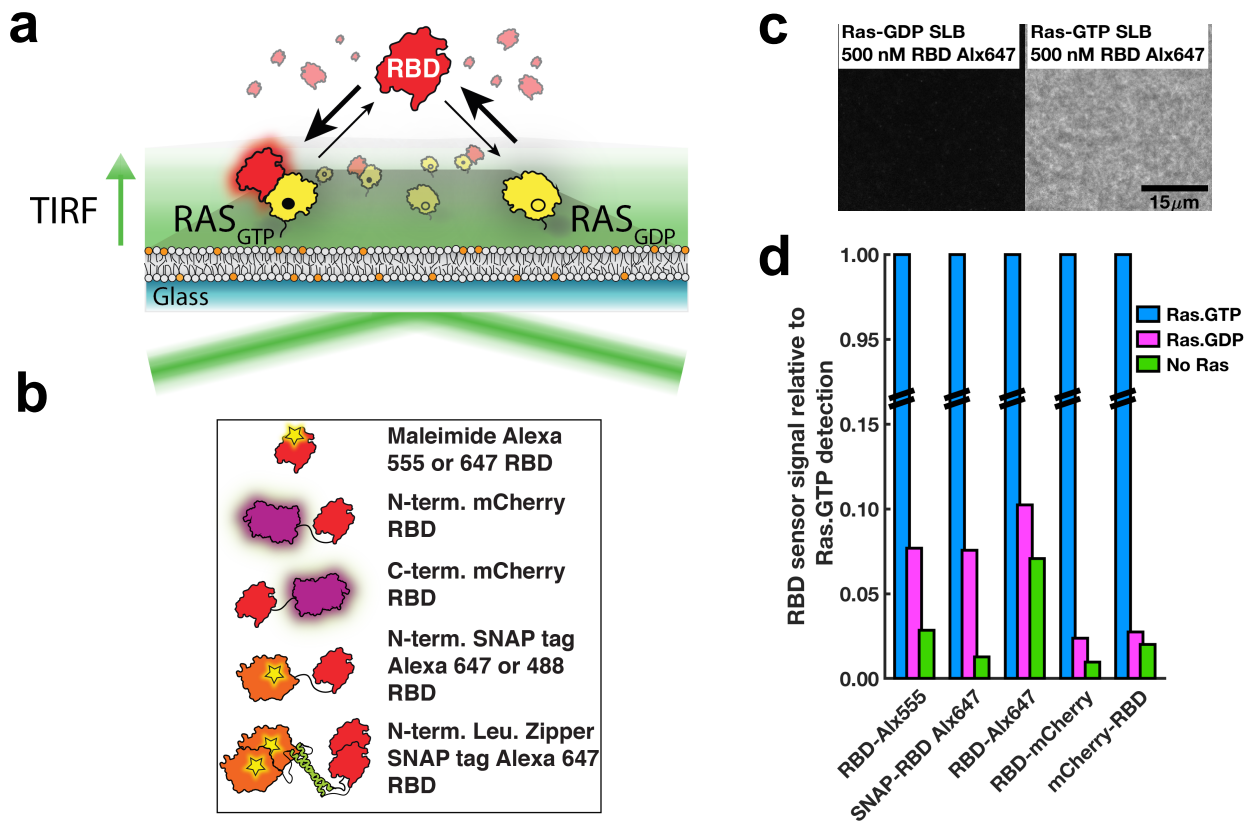

Fig. 2.1| Ras activation assay with dynamic imaging readout on supported lipid bilayers (SLBs). a, Schematic of Ras activation assay on SLBs. Ras-decorated SLBs are exposed to a solution of fluorescently labeled Ras binding domain (RBD) of Raf1. RBD preferentially binds GTP-loaded Ras (Ras-GTP) over GDP-loaded Ras (Ras-GDP). Ras activity is monitored under total internal reflection fluorescence (TIRF) illumination, limiting the excitation and detection of fluorescently labeled RBD bound to Ras-GTP and in close proximity to the membrane. **b**, Panel of RBD sensors labeled with different chemistries, fusion tags, and oligomerization states characterized in this study. **c,d** Dynamic range of active Ras detection by RBD sensors on SLBs. TIRF images of RBD binding to SLBs decorated with either Ras-GDP, Ras-GTP, or no Ras were acquired (**c**) and the mean intensity was quantified. The signal contribution of RBD sensor binding to the different surfaces is shown as a fraction of the signal from RBD sensor binding to Ras-GTP decorated SLBs (**d**). Images are displayed co-scaled (**c**). Ras densities were ~2,000 μm^{-2} (**a-d**).

An ideal sensor for Ras activation would have high specificity for binding Ras-GTP over Ras-GDP, fast equilibration kinetics, reversible binding, and short dwells. In order to develop an RBD sensor with optimal properties, we engineered a panel of RBD sensors labeled with different chemistries, fusion tags, and oligomerization states (Fig. 2.1b). RBD was labeled using Alexa 555 and Alexa 647 via maleimide chemistry, N- and C- terminal mCherry fusion

tags, N- terminal SNAP-tag, and N- terminal SNAP-tag followed by a leucine zipper(*52*) dimerization domain (SNAP-tag Leucine Zipper RBD). The dynamic range for detection of Ras-GTP over Ras-GDP was measured for sensors on the supported membrane platform (Fig. 2.1c,d). Measurements were performed under a fixed solution concentration of 500 nM RBD sensor and matched surface Ras densities. All RBD sensors displayed high selectivity for Ras-GTP, with Ras-GDP detection representing only 10% or less of the Ras-GTP detection signal (Fig. 2.1d). Small differences in Ras-GDP signal detection among the panel of sensors stem from differences in protein labeling efficiency

In contrast to the overall high specificity measured for active Ras, the panel of RBD sensors displayed differences in their unbinding kinetics (Fig. 2.2a). Ras-GTP decorated SLBs were exposed to 500 nM of RBD sensor in solution and allowed to reach equilibrium. Unbinding kinetics were measured by rapidly exchanging the solution reservoir. The resulting unbinding traces showed two predominant qualitative kinetic behaviors: biphasic unbinding, characteristic of two or multiple species (*53*) (Fig 2.2a, left panel), or single-phase, 1st order unbinding (Fig 2a, right panel). Surprisingly, only sensors with N- terminal fusion tags displayed clean 1st order desorption kinetics, suggesting that N- terminal fusion tags on RBD simplify the RBD:Ras-GTP membrane complexation kinetics.

The observed differences in sensor kinetics were further investigated by characterizing the binding (Fig 2.2b), unbinding (Fig. 2.2c), and GAP-mediated hydrolysis (Fig. 2.2d) kinetics of the N- and C- terminal mCherry fusion RBD sensors. These sensors have identical amino acid composition and differ only by the position of the mCherry fusion tag. However, their binding and unbinding equilibration kinetics and response to GAP-mediated hydrolysis show evidence of differences in the interaction of these sensors with membrane-coupled Ras-GTP that depend on the position of the fusion tag.

Binding kinetics were measured by injecting a solution with 500 nM RBD sensor to Ras-GTP decorated SLBs and measuring the approach to equilibrium. The binding traces showed differences in the equilibrium binding or signal at plateau, also consistent with the formation of an oligomeric complex for the C-terminal construct (Fig 2.2b). For experiments performed under matched sensor concentration and Ras-GTP density, the C- terminal tagged sensor reached plateau at approximately 2-times the signal observed for the N- terminal fusion sensor. Subsequently, unbinding kinetics were measured on the same samples as already described (Fig 2.2c). The resulting unbinding traces, plotted as the fraction of the maximum sensor signal at the membrane, showed a drastic difference in the fraction of sensor bound after the unbinding reaction. The fraction of bound N-terminal tagged sensor decreased by ~75%, whereas the fraction of bound N- terminal tagged sensor decreased only by ~20%. A similar modest decrease of 25% in the fraction of sensor bound was observed for the SNAP-tag Leucine Zipper RBD sensor, a stable constitutive dimer(*54*).

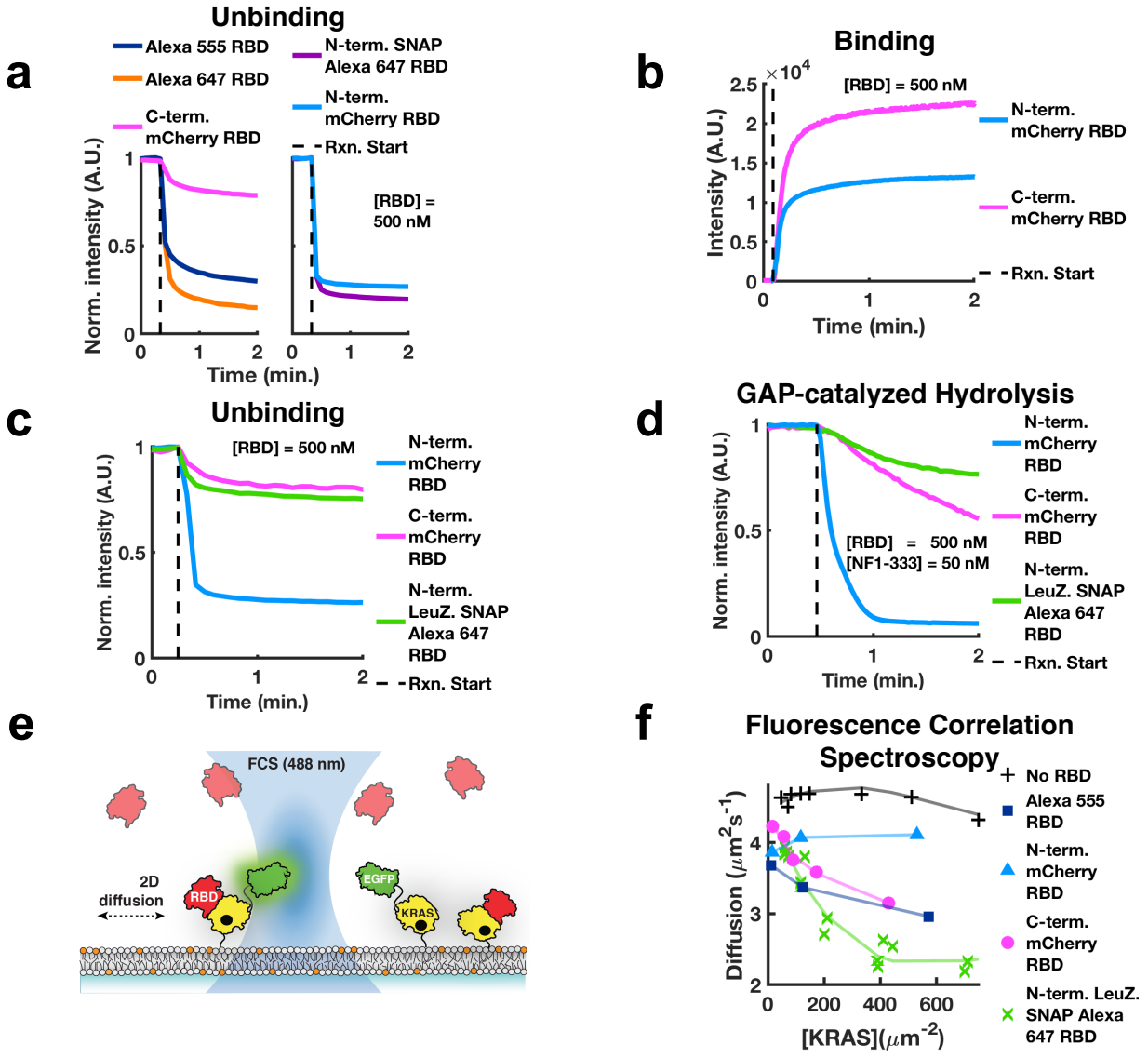

Fig. 2.2| N-terminal tagging of RBD simplifies RBD:Ras-GTP complexation kinetics on membranes. **a**, Unbinding kinetic traces of panel of RBD sensors interacting with Ras-GTP-decorated SLBs. N- terminal fusion tagged RBD sensors (right panel) displayed fast equilibration kinetics after unbinding relative to other tag positions (left panel). **b-d**, Binding (**b**), unbinding (**c**), and response to GTPase activating protein (GAP) catalyzed hydrolysis (**d**) kinetic traces for N- and C-terminal mCherry fusion tag sensors interacting with Ras-GTP decorated SLBs. These sensors have identical amino acid composition and differ only in tag position. **e**, Fluorescence Correlation Spectroscopy (FCS) experimental setup for measuring Ras membrane diffusion. **f**, FCS measurement of the effect of RBD sensors binding to Ras-GTP on Ras membrane diffusion. SNAP-tag Leucine Zipper RBD sensor, a constitutive RBD dimer, kinetic traces are included as a reference (**c-f**)

These observations are all specific to the RBD:Ras-GTP interaction. This was demonstrated by measuring the sensor response to GAP-mediated hydrolysis (Fig 2.2c). Ras-GTP decorated SLBs were incubated with 500 nM of either N- or C- terminal tagged or dimer RBD sensors, resulting in an initially high surface fluorescence intensity. Subsequently, injections with 50 nM of the catalytic domain of the GAP Neurofibromin 1 (NF1-333)(*55*) and 500 nM of RBD sensor where added to initiate the reactions. GAP-catalyzed nucleotide hydrolysis deactivates Ras, resulting in RBD unbinding and measured as a decrease in surface fluorescence intensity. The sensor response kinetics were markedly different depending on the position of the tag. The N- terminal tagged sensor showed an over 90% decrease in bound RBD sensor after one minute of the hydrolysis reaction starting. In contrast, the C- terminal tagged sensor bound decreased by only 20% at the same timepoint. This decrease is comparable to the 15% signal decrease observed for the constitutive dimer RBD sensor.

The effect of RBD sensor tag position on RBD:Ras-GTP complexation kinetics was also evident by recording changes in Ras diffusion(*56*) using Fluorescence Correlation Spectroscopy (FCS) (Fig 2.2d). In brief, FCS records the fluctuations in intensity from fluorophores coming in and out of a beam narrowly focused to a confocal volume. The time-dependent fluorescence fluctuations are analyzed with an autocorrelation function and the resulting traces are then fitted to a 2D Gaussian diffusion model from which a diffusion coefficient can be calculated.

Membrane diffusion coefficients of natively expressed and fully processed K-Ras4b(*57*) (from here on referred to as K-Ras) were quantified in the context of RBD sensor binding to GTP-loaded K-Ras. FCS measurements were performed by titrating the surface density of N-terminal eGFP tagged K-Ras in the presence of a fixed solution concentration of 250 nM of RBD sensor (with the exception of 500 nM of the SNAP-tag Leucine Zipper RBD) (Fig. 2.2e). In the absence of RBD sensor, the K-Ras membrane diffusion coefficient was measured to be ~4.5 $\mu m^2/s$ and independent of the K-Ras surface density**.** Addition of either maleimide labeled Alexa 555 RBD or C- terminal mCherry tagged RBD altered K-Ras membrane diffusion. As the K-Ras density increased, the membrane mobility decreased. The same trend, with a stronger mobility decrease, could be replicated by binding of the constitutive dimer SNAP-tag Leucine Zipper RBD sensor. Surprisingly, this effect could be disrupted by specific tagging of RBD at the N-terminus. K-Ras mobility in the presence of N-terminal mCherry tagged RBD was ~4.0 $\mu m^2/s$ and, similar to the K-Ras mobility in the absence of RBD, its mobility remained unaltered as the K-Ras surface density increased. Changing the identity of the N-terminal fusion tag for a SNAP-tag showed the same trend of unaltered K-Ras mobility. This suggests that the position of the fusion tag in the N- terminus, and not the identity, is responsible for disrupting RBD:Ras-GTP membrane oligomerization.

2.4 Optimization and characterization of N-terminal tagged RBD sensor

Having established that N- terminal fusion tags on RBD disrupt any RBD:Ras membrane oligomerization, development efforts were focused to optimizing the N- terminal SNAP-tag RBD sensor.

A good sensor should have a rapid response time (e.g. fast kinetic dissociation rate "k_{off}") and high affinity/selectivity (e.g. fast kinetic association rate "k_{on}"), allowing for a rapid readout of Ras activity state with minimal sensor presence. These properties were optimized by engineering a panel of N- terminal SNAP tag RBD sensors with a range of affinities for Ras-GTP. The RBD:Ras-GTP binding interface and the residues involved in binding have been characterized in detail(*58*). Untagged and unmodified RBD has an equilibrium dissociation constant (K_d) of 130 nM for binding Ras-GTP. Introducing point mutations K65E and T68A in RBD has been reported to decrease affinity for Ras-GTP by 5- and 10-fold, respectively, relative to the affinity of wild type RBD. N- terminal SNAP tag RBD sensor variants with either K65E or T68A point mutations were synthesized and characterized alongside the wild type (WT) RBD.

Equilibrium binding and dissociation kinetics were quantified for the panel of RBD sensors (Fig. 2.3). Ras-decorated SLBs were loaded with guanosine 5′-[β,γ-imido]triphosphate] (Gpp(NH)p) – a non-hydrolyzable analogue of GTP. Binding isotherms were generated by titrating RBD sensor solution concentration and measuring equilibrium binding to Ras (Fig. 2.3a). K_d constants were obtained by fitting the experimental data to the binding isotherm equation. Introduction of point mutations yielded sensors with affinities that generally matched previously reported values(*58*), resulting in affinities ranging from ~500 to 1,200 nM. The WT RBD sensor K_d was ~4-times higher than the reported value for untagged WT RBD, suggesting that introduction of the N-terminal fusion tag itself tunes the affinity for binding Ras-GTP. Dissociation kinetics were measured by streaming acquisitions tracking the individual motion of single RBD sensor molecules binding to Ras (Fig. 2.3b). Single-molecule dwell time distributions were reasonably well described by a single exponential equation, indicative of 1^{st}-order dissociation kinetics. The mean molecular binding dwell time ($<\tau_{off}>$), related to k_{off} by $1/<\tau_{off}>$, was obtained by mathematical fitting and correcting for photobleaching. The sensors displayed short dwell times, with $<\tau_{off}>$ that ranged from 30 to 100 ms.

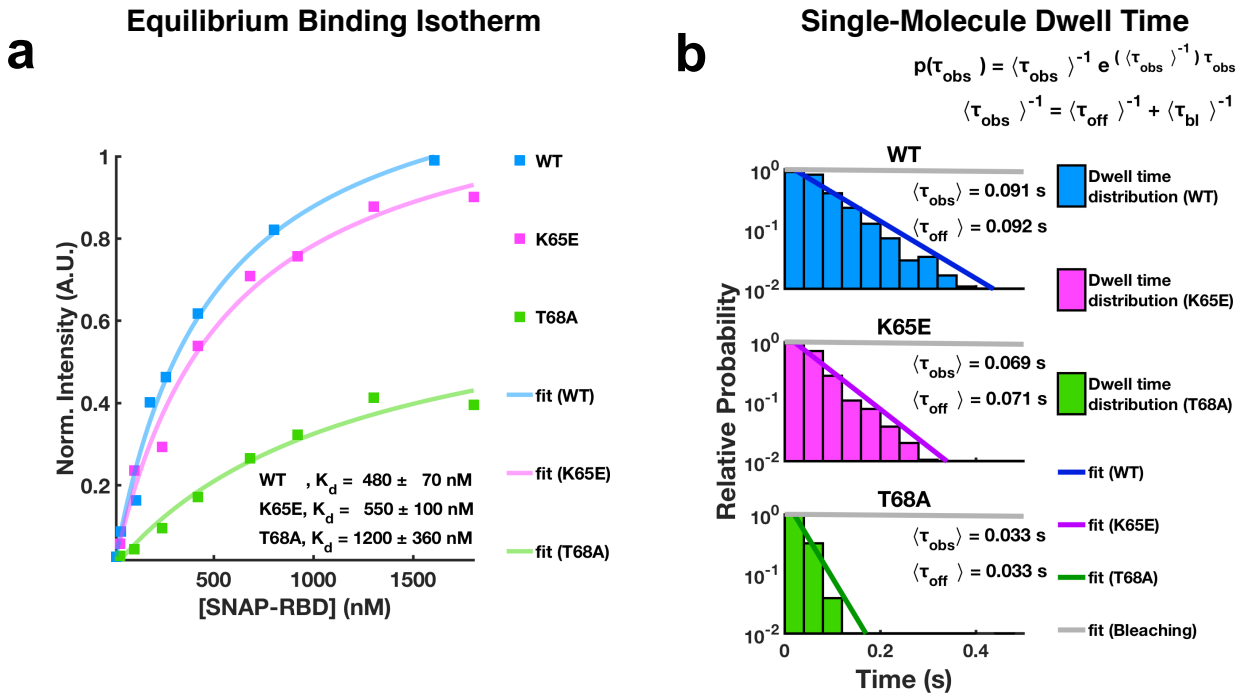

Fig.2.3| Optimization and characterization of N-terminal tagged SNAP-RBD sensor. **a**,**b**, Characterization of panel of N-terminal tagged SNAP RBD sensors on Ras-decorated SLBs loaded with the non-hydrolysable GTP analogue, Gpp(NH)p. Equilibrium binding isotherms (**a**) and single-molecule dwell-time distributions (**b**) of wild type (WT; n=13,722), K65E (n = 10,654) , and T68A (n=7,045) SNAP-RBD Alexa 647 sensors. Dwell times were measured with streaming acquisitions at 95 Hz.

Overall, the panel of sensors retained a relatively high affinity for Ras-GTP and fast dissociation kinetics. Given the similar kinetics measured between the WT and K65E sensors, subsequent characterization focused on only one sensor, the K65E mutant.

2.5 Real-time readout of Ras activation and deactivation on supported membranes

The N- terminal SNAP tag RBD sensor was characterized in the context of reporting Ras activation by GEF-mediated nucleotide exchange, GAP-catalyzed Ras deactivation by nucleotide hydrolysis, and dynamic Ras switch cycling in GAP/GEF competition reactions (Fig. 2.4). Concurrent sampling of hundreds reactions was achieved by reconstituting the Ras-supported bilayer platform on substrates patterned with micrometer scale chromium grids(*59*). These lithographically defined and chemically inert barriers constrain the lateral diffusion of the membrane-associated components without affecting the adjoining solution,

effectively partitioning the membrane into hundreds of reactions exposed to the same enzyme solution input.

The effectiveness of the N- terminal SNAP tag RBD sensor in reporting Ras activation by nucleotide exchange was determined by simultaneously measuring nucleotide release and RBD sensor binding to Ras-GTP (Fig. 2.4a). Ras-decorated SLBs were loaded with Atto 488-labeled fluorescent nucleotide 2′/3′-O-(2-aminoethyl-carbamoyl)-guanosine-5′-diphosphate (Atto488-EDA-GDP, and from here on referred to as Atto488-GDP), resulting in an initial high surface fluorescence intensity. The nucleotide exchange reaction was initiated by injection of a solution of 20 nM SOS_{cat}, 1 mM GTP, and 50 nM Alexa 647 labeled RBD sensor. We used dual color TIRF microscopy to simultaneously measure changes in surface fluorescence intensity from fluorescent nucleotide release from Ras and from RBD sensor binding Ras-GTP. The resulting nucleotide exchange and RBD sensor binding traces show a sigmoidal response, further evidence of the Ras-GTP and SOS positive feedback loop(*24*), and essentially mirror each other (Fig. 2.4b, bottom panel). The Ras activation kinetics reported by the RBD sensor were benchmarked against the nucleotide exchange readout by inverting individual RBD sensor traces and subtracting its corresponding nucleotide exchange trace (Fig. 2.4b, top panel). On average, the difference in reporting nucleotide exchange between the RBD sensor and labeled nucleotide is less than 10 %.

In addition to reporting Ras activation by nucleotide exchange on Ras, the RBD sensor can report Ras deactivation by nucleotide hydrolysis (Fig. 2.4c). To our knowledge, alternative probes for measuring the dynamics of nucleotide hydrolysis that are compatible with TIRF microscopy and could be implemented simultaneously with the RBD sensor are not available. Therefore, we characterize the RBD sensor as a readout of nucleotide hydrolysis by showing its sensitivity in reporting the distinct activities of two GAP enzymes, the catalytic domains of NF1 and p120 GAP (*60*) (p120-334).

Ras-decorated SLBs were reconstituted on patterned substrates, initially loaded with GTP, and incubated with 50 nM RBD sensor to measure the initial density of Ras-GTP. The enzyme-catalyzed hydrolysis reaction was then initiated by injection of GAP enzyme and 50 nM RBD sensor. The resulting traces show the RBD sensor response to the distinct activities and concentrations of NF1-333 and p120-334 (Fig. 2.4d). NF1-333 and p120-334 have been measured to have a similar catalytic rate constants (k_{cat}) of ~ 8 s^{-1}, but differ in their Michaelis-Menten constant (K_M) by approximately 22-fold, 0.23 μM and 5 μM respectively (*61*). This difference in K_M was evident in the responses reported by the RBD sensor. For a 500 nM solution concentration of p120-334, only ~20 % of the hydrolysis reaction had gone to completion after 1 minute. Doubling the concentration of p120-334 to 1000 nM has a linear effect on the reaction rate, reaching ~40% completion at the same timepoint. In contrast, for a 20-times lower solution concentration NF1-333, the hydrolysis reaction went to 100 % completion in less than 1 minute.

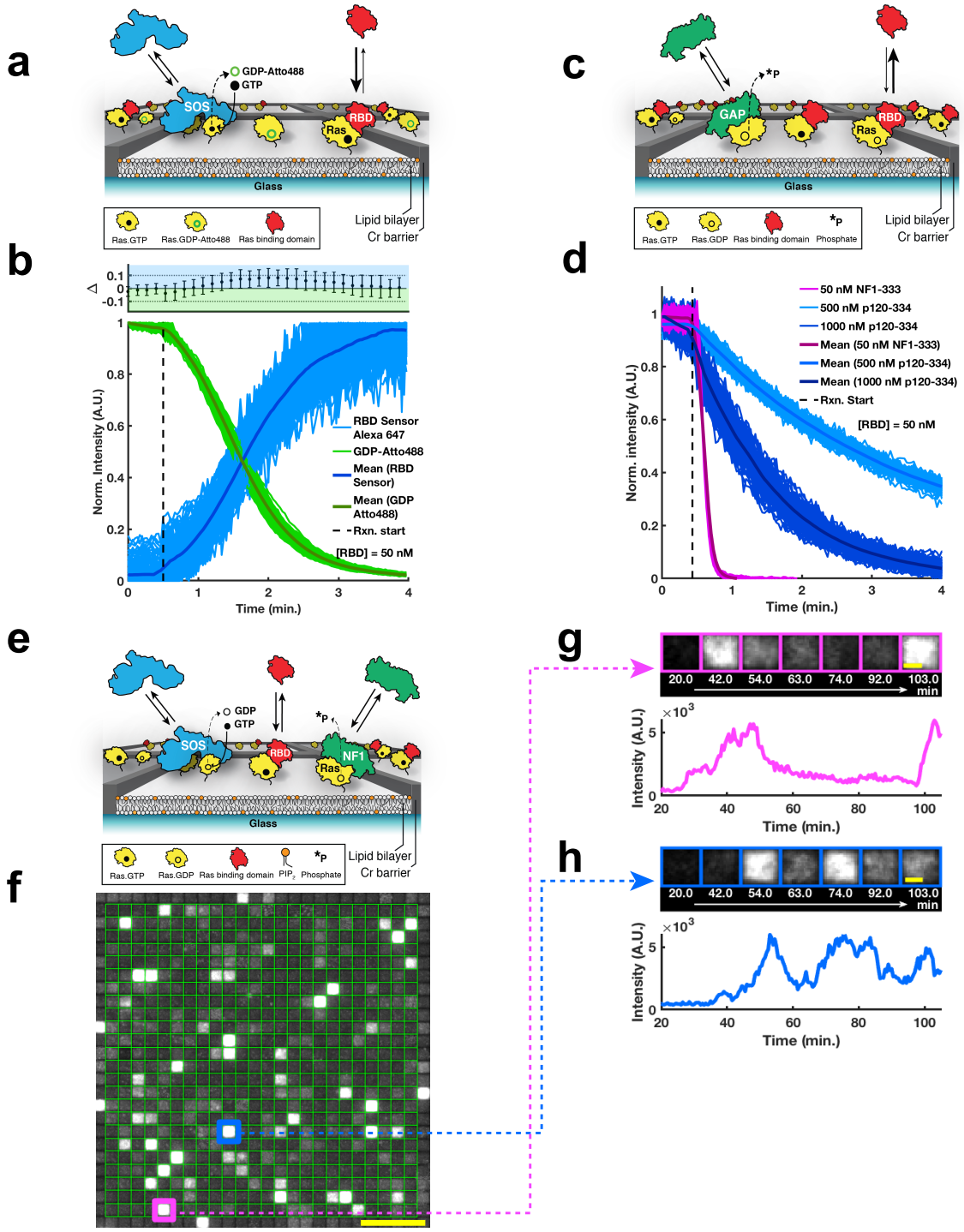

Fig. 2.4| N- terminal SNAP tag RBD sensor is a reversible and dynamic readout of Ras activation state. **a,** Experimental setup for dual readout GEF catalyzed nucleotide exchange assay. Nucleotide exchange reaction catalyzed with 20 nM of the catalytic domain of SOS (SOS_{cat}) is monitored by simultaneously measuring GDP-Atto488 nucleotide release and RBD sensor binding. **b,** Plot of fluorescent

nucleotide release and RBD sensor recruitment (bottom panel) and difference in signals reported between probes (top panel; n=144, mean ± s.d.). **c,** Experimental setup for GAP-catalyzed hydrolysis assay. **d,** Plot of resulting traces from nucleotide hydrolysis catalyzed by different concentrations of the catalytic domains of NF1 (NF1-333) and p120 (p120-334) GAP enzymes. **e,** Experimental setup for dynamic readout of Ras activation in GAP and GEF competition reactions. **f,** 2-Dimensional maximum intensity projection of timelapse monitoring corralled competition reactions of 500 pM NF1-333 and 2 nM of SOS_{HDPC} – an autoinhibited and truncated SOS construct lacking the proline rich domain. **g,h**, Plots of Ras activation dynamics and sample images for a subset of corralled reactions. Reactions were reconstituted on microfabricated substrates patterned with chromium grids, enabling simultaneous sampling of ~150 (**a-d**) or ~600 reactions in a single field of view (**e-h**). Scalebars are 10 μm (**f**) and 1 μm (**g,h**).

The RBD sensor is a reversible and multi-turnover readout of Ras activation state. This makes the RBD sensor a unique probe in that it can dynamically report the cycling of Ras in simultaneous GAP and GEF competition reactions (Fig. 2.4e). Samples were prepared on patterned substrates as previously described for the nucleotide exchange assay, with the exception that Ras is initially loaded with GDP and PS lipids were replaced with phosphatidylinositol 4,5-bisphosphate (PIP_2). The reaction was initiated with an injection of 1 mM GTP, 500 pM NF1-333, and 2 nM of SOS_{HDPC} – an autoinhibited and truncated SOS construct lacking the proline rich domain. Simultaneous measurement of over 500 reactions exposed to the same enzyme solution input reveals broad heterogeneity in the dynamics of individual reactions (Fig. 2.4e). Stochastic and spatially uncoupled pulses in Ras activation were observed in corralled reactions (Fig. 2.4f,g). Heterogeneity in the dynamics of Ras activation likely stems from processivity and stochastic fluctuations in SOS activity(*28*).

2.6 Discussion

Here, we have established a biochemical assay that enables the study of Ras dynamic cycling in the context of a membrane. We extended the *in vitro* reconstitution of Ras on supported membranes to include a multi-turnover, real-time, fluorescence imaging readout of Ras activation state based on the RBD of Raf1. This approach enables quantification of Ras activation, deactivation, and dynamic cycling kinetics with precise control over membrane input parameters.

Characterization of the RBD interaction with Ras-GTP on supported membranes was essential in developing a faithful reporter of Ras activity. We observed that, while RBD has high specificity for Ras-GTP over Ras-GDP, it displayed intricate complexation kinetics. RBD showed slow unbinding kinetics from Ras-GTP and, consistent with previous reports(*62*, *63*), it sequestered active Ras from GAP-mediated hydrolysis. We also observed that RBD binding to Ras-GTP decreased lateral diffusion of Ras on membranes in a Ras density dependent manner. We discovered that N- terminal tagging of RBD simplifies RBD:Ras-GTP complexation kinetics; this sensor showed fast unbinding kinetics, minimal interference with GAP-mediated hydrolysis, and does not alter Ras membrane diffusion as Ras density increases. Furthermore, it retains a relatively high affinity for Ras-GTP, with an approximate

K_d of 500 nM, and dwells on its substrate on average for less than 100 ms. We demonstrated that using this sensor at a solution concentration 10-times below the K_d, where the fractional occupancy of Ras is approximately 10 %, it can report nucleotide exchange kinetics with ~90 % accuracy and is sensitive to the activity of different GAPs.

In vitro biochemical assays that better approximate the membrane context of Ras signal transduction in cells have the potential of uncovering novel features of Ras function. The assay and sensor presented here provide a platform to bottom-up reconstitute multi-component Ras signaling networks on supported membranes. The reconstitution approach is unique in that, in addition to reporting Ras activation state in real-time, it enables examination of protein-protein and protein-membrane interactions with molecular detail and high spatiotemporal resolution. With precise control over parameter space, this assay gives access to multiple aspects of Ras function, including spatial organization, bimolecular interactions with effectors, regulation by enzymes, modulation by signaling complexes, perturbations by mutations, and complex membrane-dependent feedback mechanisms. We anticipate that this reconstitution platform will be complimentary to top-down approaches and techniques that interrogate living cells, enabling the investigation of molecular models and dissection of regulatory mechanisms otherwise inaccessible from other assays. We also expect that extending this assay to high-throughput format facilitates drug screening of Ras on membranes.

Chapter 3

Processive SOS activity is not uniquely determined by allosteric Ras binding

This chapter is part of a manuscript in preparation co-first authored by S. Alvarez and H.Y.M. Lam.

3.1 Abstract

Activation of the guanine nucleotide exchange factor Son of Sevenless (SOS) is a key step in controlling Ras signaling. SOS has a multidomain architecture comprised of a catalytic subunit flanked by regulatory domains. It is highly autoinhibited in solution and achieves full activation through specific interactions, such as lipid and allosteric Ras binding, at the cell membrane. SOS is capable of accessing a long-lived, highly processive state that can activate up to hundreds of Ras molecules. Thus, a detailed, molecular understanding of full SOS activation is essential. We describe the receptor-independent *in vitro* reconstitution of Ras activation by SOS on supported lipid bilayers. Imaging of single molecule SOS recruitment and Ras activation detected using the Ras binding domain (RBD) of Raf1, on micropatterned membranes enables correlating SOS membrane localization with Ras activation in hundreds of reactions simultaneously. We found that SOS activates Ras with two distinct kinetics: switch-like activation, referred to as burst activation, and gradual activation, referred to as transient activation. We demonstrate that burst activity, in which maximal Ras activation is reached with a sudden, steep transition, is the result of long-dwelling, stably-recruited single molecules of SOS. Both burst and transient SOS activities are modulated by the density of active Ras on the membrane, suggesting that a structural rearrangement at the membrane, rather than allosteric Ras binding, is responsible for the distinct kinetic states. Furthermore, regulatory domains of SOS suppress transient activity while retaining the burst activity, arguing that burst activity might be the signaling competent kinetic state in the cell context. Structural rearrangements at the membrane and release of autoinhibition likely represent kinetic proofreading steps that modulate full SOS activation and, ultimately, MAPK signal propagation.

3.2 Introduction

Ras is a membrane-anchored guanosine triphosphatase (GTPase) protein that serves as a hub to signaling pathways in control of essential cellular functions and often mutated in cancer. Ras function resembles a switch; inactive when bound to guanosine diphosphate (GDP) and active when bound to guanosine triphosphate (GTP)(*64*). The activation state of Ras is tightly controlled by regulatory enzymes that catalyze the interconversion between "ON" and "OFF" states. Guanine nucleotide exchange factors (GEFs) activate Ras by catalyzing the exchange of GDP-to-GTP, while GTPase activating proteins (GAPs) catalyze the hydrolysis of GTP-to-GDP (*10*, *39*). Perturbations to Ras, GAPs, and GEFs can have deleterious consequences and are the root of many types of cancers and developmental disorders(*45*, *65*).

Son of Sevenless (SOS) is a ubiquitously expressed(*11*) Ras GEF and a key gatekeeper in control of Ras signal propagation from membrane receptors. An allosteric mechanism in SOS has been implicated in the switch-like responses downstream of T-Cell receptor(*27*) and sustained ERK kinase signaling downstream of the epidermal growth factor (EGFR)(*66*), underscoring the essential role of SOS in Ras signaling dynamics and discreet biological outcomes.

Receptor-mediated Ras activation by SOS is a process compounded by multiple layers of regulation that are predicted to ensure signal fidelity(*47*). Regulation in SOS begins with its multidomain structure (Fig 3.1a). SOS is comprised of a catalytic core that has a Ras exchanger motif (REM) and a Cdc25 domain, flanked by a proline rich (PR) C- terminal domain and histone-fold (HF), plecksterin homology (PH), and Dbl homology (DH) N-terminal domains(*12*). The N- and C- terminal regulatory regions contribute to an autoinhibited conformation of the enzyme(*13*–*15*), predicted to be the predominant state of SOS in the cytosol. The activation of cell surface receptors induces the translocation of SOS to the plasma membrane, where it can efficiently encounter substrate Ras. The adaptor protein Grb2 mediates SOS translocation to the membrane by bridging SOS to phosphorylated tyrosines on membrane receptors and scaffold proteins(*1*, *16*–*21*). Once in the proximity of the membrane, interactions of the N- terminal domains with membrane lipids relieve SOS autoinhibition and expose the catalytic core(*13*, *22*, *23*, *25*). As a result, a distal Ras binding site interposed between the Cdc25 and REM binds active Ras and allosterically activates the catalytic site(*24*), resulting in SOS activation. Collectively, the multiple interactions of the N- and C- terminus of SOS at the membrane surface and allosteric Ras binding are predicted to act in concert to relieve autoinhibition and activate SOS(*25*, *26*).

The allosteric activation of SOS has profound implications in Ras signaling. The allosteric pocket has a 10-fold higher affinity for GTP-bound Ras (Ras-GTP) over GDP-bound Ras (Ras-GDP)(*13*), introducing positive feedback in Ras activation and signal amplification(*22*, *27*, *66*). However, the specific nature of this positive feedback remains an

area of ongoing research. The allosteric activation of SOS has been traditionally rationalized to originate from the nucleotide-specificity in allosteric Ras binding. This was contested by experiments resolving the activity of single enzymes of SOS showing that mean catalytic rates are largely unaltered by the activation state of allosteric bound Ras(*28*). Recent work suggests an alternative mechanism for establishing positive feedback from allosteric SOS activation. Binding of Ras in the allosteric site has been shown to be sufficient to recruit and anchor SOS to membranes, with Ras-GTP increasing the probability SOS recruitment(*22*, *29*). Single-molecule reconstitution measurements of SOS activity showed that SOS can dwell on membranes for extended periods, up to minutes, and processively activate thousands of Ras molecules in a single residency period (*29*). The single-molecule activity traces showed that SOS samples a broad spectrum of turnover rates by stochastically fluctuating between long-lived functional states, including highly active processive states(*28*). These highly processive states have been observed in a range of SOS constructs *in vitro*, from the minimal catalytic core to the full-length protein(*15*, *28*), suggesting it is an bona fide feature of this GEF and potentially a functional state of SOS in the cellular context. Altogether, these observations are suggestive of a positive feedback mechanism where allosteric activation of SOS enables access to highly active processive states, with the potential of amplifying and driving forward signal propagation from Ras.

The structural basis, allosteric regulation, and key defining features in SOS that control access to these highly active processive states are yet to be resolved. Here, we developed a receptor-independent SOS activation assay where we resolved the recruitment and activity of single molecules of SOS anchored predominantly by allosteric Ras binding. By implementing a membrane micropatterning strategy, we simultaneously measured Ras activation in hundreds of reactions exposed to the same adjoining solution input. Reaction trajectories displayed two prevalent kinetic behaviors: a gradual increase in Ras activation experienced by all the reactions, as well as stochastic sharp transitions in activity superimposed to the gradual increase in activity. Close examination of the two distinct kinetic behaviors revealed that the gradual activation was a result of short-dwelling transient SOS activity, while bursts in Ras activation were a result of solution-recruited and long-dwelling single molecules of SOS processively activating Ras. Both activities in SOS were shown to be sensitive to the density of Ras-GTP, indicative of allosteric Ras engagement in both states. This suggests that the transition from transient-to-processive activation states is not uniquely determined by allosteric Ras binding and is potentially a result of a distinct structural conformation. The full-length SOS protein largely suppressed the transient activation and only displayed processive “burst” activity, further supporting that this might be the competent signaling state of SOS in cellular context.

3.3 SOS recruitment and activation assay on supported membranes

We developed an imaging assay to simultaneously measure the membrane recruitment of single-molecules of SOS and its nucleotide exchange activity on membrane-coupled Ras (Fig 3.1c). SLBs consisting of 94% EGG-PC (L-α-phosphatidylcholine), 3% PIP2, and 3% MCC-DOPE{1,2-dioleoyl-sn-glycero-3-phosphoethanolamine-N-[4-(p-maleimidomethyl) cyclohexane-carboxamide]} were deposited on glass substrates by vesicle fusion. H-Ras (from here on referred to as "Ras") was covalently attached to membranes via maleimide chemistry with the MCC-DOPE lipids. Membrane-coupled Ras retained lateral mobility and densities were measured to be ~2,000 μm^{-2}, comparable to the >1,000 μm^{-2} densities reported for Ras clusters in cells(*46*, *50*, *51*). Ras-decorated SLBs were reconstituted on substrates patterned with 2-by-2 μm chromium grids. The lithographically defined and chemically inert barriers restrict 2-dimensional lateral diffusion of membrane components without perturbing the adjoining solution. This method effectively partitions the membrane into hundreds of reactions that are exposed to a common solution input and can be measured simultaneously. Single molecule SOS recruitment and Ras activation were measured by detecting the binding of fluorescently labeled proteins to Ras-decorated membrane surfaces using total internal reflection microscopy (TIRFM). Real time Ras activation was achieved by recording the rapid and reversible binding of a Ras binding domain (RBD) sensor to membrane-coupled Ras. This sensor, based on the RBD of Raf1 kinase and with natural high affinity for Ras-GTP, was engineered to remove a previously unknown tendency to oligomerize on membranes and optimized for reporting Ras activation on membranes (discussed in Chapter 2).

In a typical experiment, Ras-decorated SLBs reconstituted on micropatterned substrates were preloaded with GDP to ensure all Ras is initially in its inactive state (Fig 3.1c). The GDP-bound state of Ras was confirmed from the equilibrium binding of the RBD sensor, were sensor binding signal was minimal. Reactions were initiated by injection of a solution of GTP, RBD sensor, and SOS and maintained at a constant concentration throughout the experiment. Reaction progress was monitored by dual color TIRFM, where both SOS and RBD sensor membrane recruitment were quantified. Ras density per corralled reaction was determined at the end of each experiment by driving the Ras-decorated surface to full activation and measuring RBD sensor binding. A calibration curve obtained from fluorescence correlation spectroscopy (FCS) enabled determining the local Ras density from the fluorescence intensity signal from RBD sensor binding (see Appendix A.6).

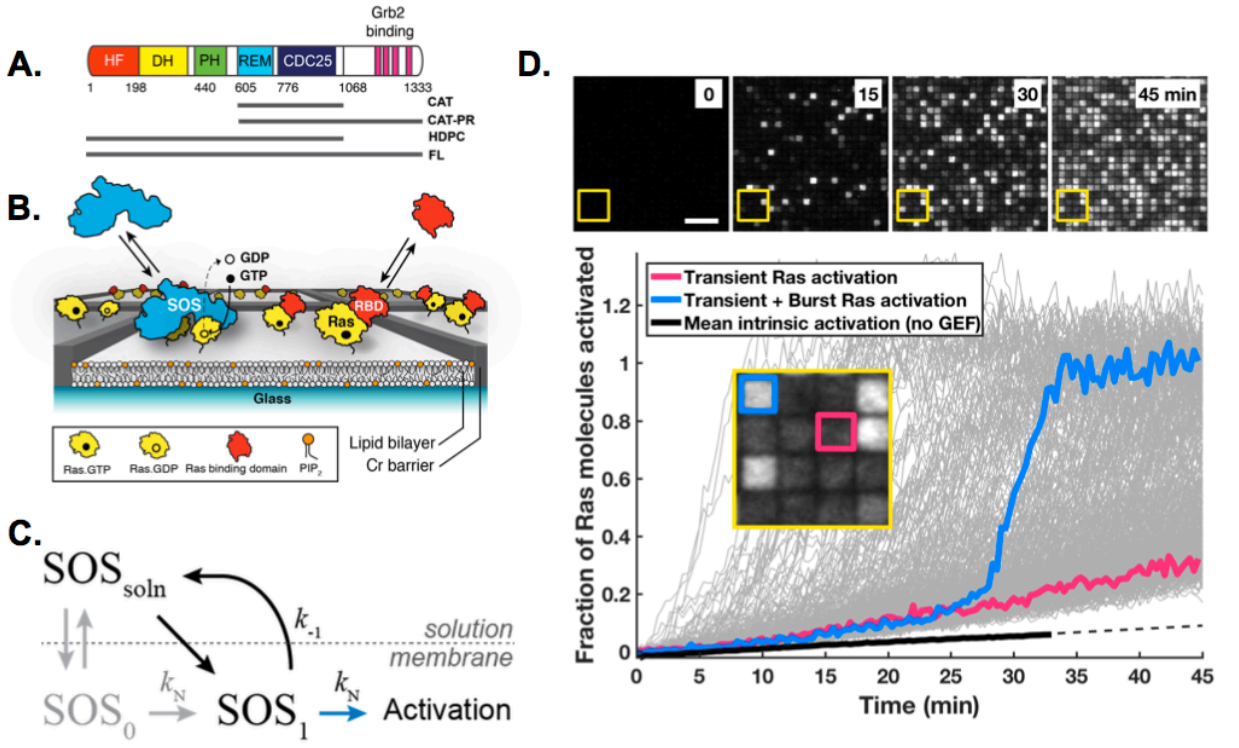

Fig. 3.1| Receptor-independent single-molecule activation assay of SOS on supported membranes. **A,** Domain organization of SOS. **B,** Schematic of receptor-independent SOS activation assay. H-Ras preloaded with GDP is tethered to supported membranes corralled by 2 x 2 μm chromium grids. SOS- Alexa Flour 647, SNAP-RBD (K65E)-Alexa Flour 488, and GTP are injected to initiate the reaction. Single-molecule SOS recruitment and Ras activation are simultaneously measured by TIRF microscopy. **C,** In the absence of Grb2 and activated receptor, SOS is recruited to the membrane by allosteric Ras binding and lipid interactions *in vitro*. **D,** Ras activation by SOS^{HDPC} . Real time reaction progress (top; 10 μm scale bar). Quantification of Ras activation (below).

3.4 SOS^{HDPC} displays two distinct activities on membranes

We first explored the recruitment and nucleotide exchange activity of SOS^{HDPC} (Fig 3.1a) – an autoinhibited SOS construct lacking the C-terminal Grb2 binding domain. Simultaneous sampling of hundreds of reactions showed that, despite being exposed to a common enzyme solution input, individual reactions progressed with a high degree of heterogeneity (Fig 3.1d, montage images). Close inspection of the reaction trajectories, quantified from the mean pixel intensity per corral, revealed two predominant qualitative behaviors: a gradual increase in Ras activation (Fig. 3.1d, magenta trace), as well as sharp and steep transitions in Ras activation (Fig. 3.1d, blue trace). Both of these activities are the result of GEF catalysis; their rates of activation are above the slow and linear rate of Ras intrinsic nucleotide exchange measured in the absence of GEF (Fig. 3.1d, black trace).

The gradual increase in Ras activation was observed in all the corralled reactions and, after a 45 min acquisition, contributed to the activation of ~30 % of the total Ras per corral. The narrow deviation from the mean activation rate for all the reactions displaying this gradual increase in activity (Supplementary data) suggests that all corrals experienced a similar catalytic activity from SOS. This suggests that this activity is potentially the result of transient interactions of SOS with membrane-coupled Ras, were membrane binding results in only one or few turnovers events (from here on referred to as "transient Ras activation ").

A subset of the corralled reactions showed sharp and steep transitions in progress curves that were superimposed to the transient Ras activation observed in all reactions. The onset of these transitions was stochastic and would often drive the reactions to full Ras activation within minutes of the onset. Imaging of SOS recruitment revealed that the onset of these bursts in Ras activation (from here on referred to as "burst Ras activation") corresponded with the solution recruitment and stable membrane association of single molecules of SOS (Fig. 3.2A). These long-dwelling single SOS^{HDPC} molecules could be observed anchored to the membrane for minutes (Fig. 3.2A, montage) and processively activating hundreds of Ras molecules (Fig. 3.2A, trace). Bursts in Ras activation resulting from the recruitment of long-dwelling single SOS enzymes were also observed in the context of competing reactions, where the catalytic domain of the GAP Neurofibromin 1 (NF1-333) catalyzes nucleotide hydrolysis and opposes SOS activity (Fig. 3.2B). In this context, the transient Ras activation by SOS was suppressed. However, membrane recruitment of long-dwelling single SOS molecules overcame the negative GAP pressure and processively activated Ras. The onset of the burst in Ras activation coincided with the dwell of the SOS molecule; membrane detachment of the single SOS enzyme enabled the GAP negative pressure to dominate the reaction.

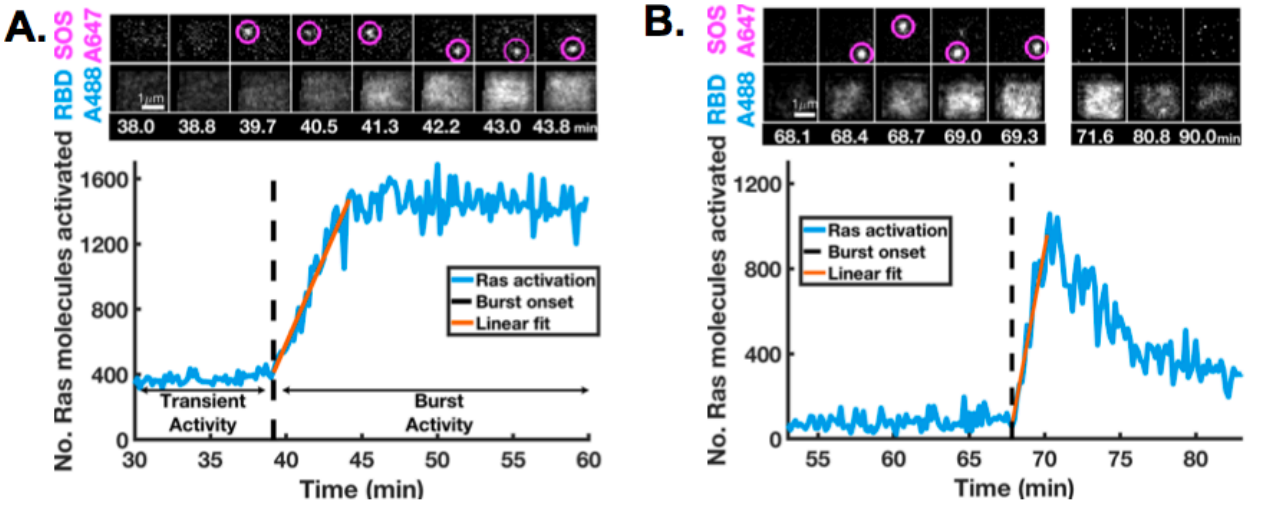

Fig. 3.2| A single molecule of SOS can processively activate hundreds of Ras molecules. A) Representative example of the recruitment of a single molecule of SOS^{HDPC}, resulting in a steep transition in Ras activation (data, top panel; quantification, bottom panel). **B**) Ras activation by SOS^{HDPC} in the presence of the catalytic domain of the GTPase activating protein, Neurofibromin 1 (NF1-333)

3.5 Transient and Burst SOS activities involve allosteric Ras binding

Burst Ras activation is mediated by long-dwelling SOS molecules that are anchored to the membrane predominantly by allosteric Ras binding. This was demonstrated by Christensen and colleagues(*29*) who analyzed the time-integrated membrane recruitment of SOS^{cat} – the minimal catalytic unit of SOS with two binding pockets for Ras, catalytic and allosteric sites, and lacking any lipid-binding domains (Fig. 3.1A). Christensen and colleagues employed a pulse-chase method to study SOS^{cat} recruitment, where a solution containing SOS^{cat} is transiently pulsed over Ras-decorated bilayers and followed by a chase with a nucleotide solution. The probability of SOS engaging Ras is quantified by directly counting the membrane-anchored and catalytically active single molecules of SOS present after the chase. Using this approach, they observed a 16-fold enhancement in the stable membrane recruitment of SOS^{cat} when binding Ras-GTP versus Ras-GDP. The catalytic site of SOS is insensitive to the identity of nucleotide bound to Ras(*67*, *68*), whereas the allosteric site has a higher affinity for Ras-GTP(*13*). Therefore, the recruitment enhancement by Ras-GTP suggests that membrane anchoring of long-dwelling SOS molecules is predominantly mediated by allosteric Ras binding and underscores a critical role of allosteric Ras binding in mediating SOS processive activity.

We hypothesized allosteric Ras binding to be the key defining feature controlling access to SOS processive state. This implies that the transient activity observed in SOS^{HDPC} (Fig. 3.1D) does not engage Ras in the allosteric site and only involves the catalytic site. In this scenario, transient Ras activation would stem from short membrane dwells of SOS that are mediated by the catalytic site and result in one or few turnover events. Thus, the transition from transient-to-processive activity in SOS would be uniquely determined by allosteric Ras binding. To test this hypothesis, we set out to determine if the transient Ras activity displayed by SOS^{HDPC} is sensitive to Ras-GTP and consequently involves allosteric Ras binding (Fig. 3.3). The sensitivity of the transient SOS activity was determined by reconstituting Ras-decorated SLBs on micropatterned substrates, where the initial amount of Ras-GTP present prior to initiating the reaction was tuned (Fig 3.3a). Because of the distinct signatures between transient and burst reaction trajectories, we were able to classify reactions according to the type of activity. The effect of Ras-GTP in transient SOS activity was measured by quantifying an effective rate constant (k_{eff}) over the course of the first 10 minutes of the reactions (Fig 3.3b). The distributions of k_{eff} measured for SOS^{HDPC} show an ~10-fold increase in the mean k_{eff} for reactions doped with 58% Ras-GTP in comparison to samples with no Ras-GTP (Fig 3.3c). Therefore, allosteric Ras binding is also involved in the transient SOS activity and not unique to SOS processive activity.

Allosteric activation in full-length SOS (SOS^{FL}) (Fig. 3.1A) has not been previously studied due to challenges with of purification the full-length protein, which have only been recently overcome(*47*). Thus, we tested if the observations made for the modulation of

transient activity in SOS^{HDPC} by Ras-GTP would also hold for the full-length protein. Transient activity was largely suppressed in SOS^{FL} and showed low sensitivity to the initial Ras-GTP density, as demonstrated by the overlapping k_{eff} distributions before and after Ras-GTP doping (Fig. 3.3D). The suppression of the transient activity in SOS^{FL} is likely contributed by the C- terminal domain of SOS, which has been recently reported to contribute to enzyme autoinhibition(*15*, *29*).Despite the suppression in transient activity, SOS^{FL} activity showed bursts in Ras activation.

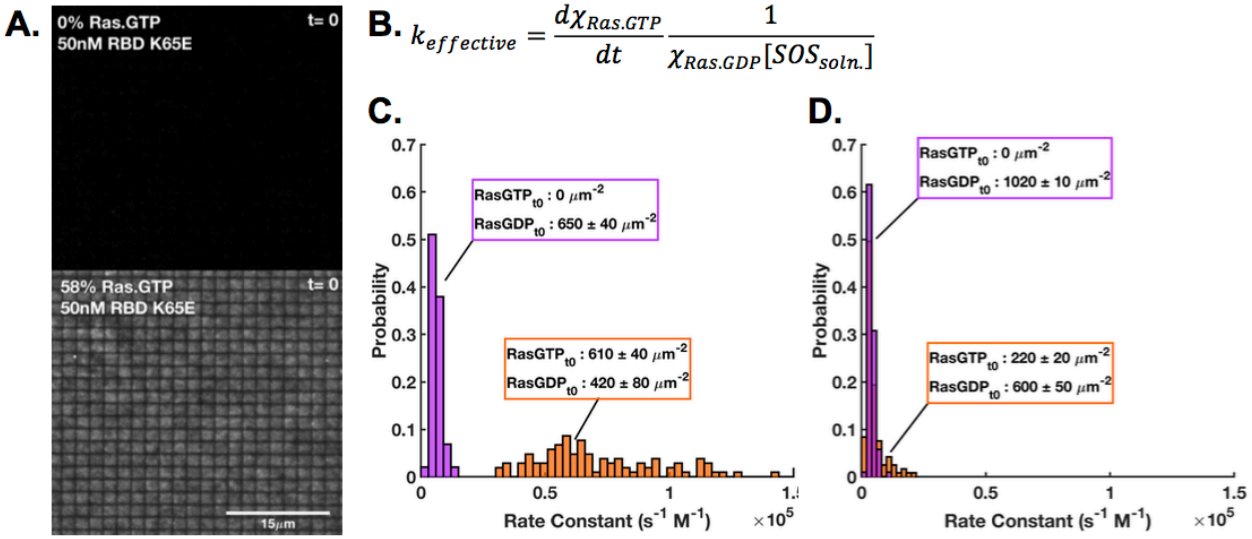

Fig. 3.3| Allosteric Ras binding is not unique to processive SOS. A) Starting amount of active Ras is tuned prior to initiating the reaction. TIRF images of corralled Ras decorated supported membranes preloaded with GDP (top) or doped with GTP (below). **B)** Effective rate constant equation for transient SOS activity in solution. **C)** Transient SOS^{HDPC} activity is modulated by the density of active Ras. **D)** Transient SOS^{FL} activity, fully autoinhibited in solution, is insensitive to the density of active Ras.

3.6 Allosteric Ras-GTP binding increases the probability of SOS processivity

Given the role of allosteric Ras binding in anchoring SOS to the membrane (discussed in section 3.4), we hypothesized that positive feedback could arise from allosteric Ras-GTP binding modulating the probability of SOS entering the processive state. We quantified the rate of Ras burst activation for SOS^{HDPC} and for SOS^{FL} (Fig. 3.4). Reaction trajectories displaying Ras burst activity were isolated and the burst onset was identified using a changepoint algorithm (Fig. 3.4A). The probability per second or rate of activation was calculated by determining the number of changepoint events per number of Ras-GTP molecules on the membrane relative to the residence time of all reactions (see Appendix B.1). The rate distributions for both the activation of both SOS^{HDPC} and SOS^{FL} show an

increase in the rate of burst events as the amount of Ras-GTP increases (Fig. 3.4 C, D). This indicates a positive modulation of burst activation by allosteric Ras-GTP binding.

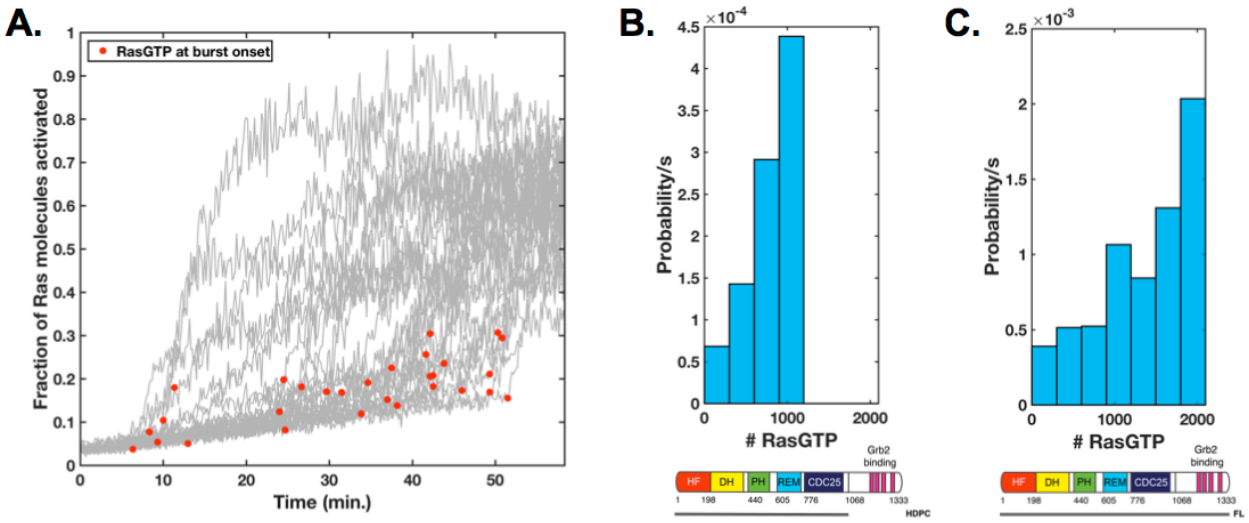

Fig. 3.4| Allosteric binding of Ras-GTP increases the probability of SOS processivity: a potential mechanism for establishing positive feedback. A) Reactions showing burst activation are isolated and transition points are identified. Transient SOS^{HDPC} activity is modulated by the density of active Ras. **B,C**) Probability of (**B**) SOS^{HDPC} and (**C**) SOS^{FL} entering the processive state as a function of Ras-GTP density.

3.7 Discussion

Recent work reconstituting SOS activity *in vitro* and in living cells has revealed novel features in the allosteric activation of SOS (*15*, *28*, *29*), adding new dimensions to our understanding of SOS function and with potential implications in Ras signal amplification. SOS anchoring to membranes by allosteric Ras binding, processive activity, and dynamic fluctuations into highly active states could provide the basis for positive feedback. How SOS accesses these highly active processive states, from fully-autoinhibited to membrane anchored, and the role of allosteric regulation in this process are yet to be determined.

The reconstitution of receptor-mediated SOS activation was recently achieved(*47*), enabling the transition from fully-autoinhibited solution state to membrane-anchored processive state be resolved. In this context, SOS membrane anchoring is driven by Grb2, membrane lipids, and allosteric Ras binding. Although a more complete reconstitution, this approach confounds the multiple surface inputs mediating SOS processivity and complicates isolating the role of allosteric Ras binding in SOS state transitions. The assay presented here resolves the recruitment and activity of single molecules in the absence of receptor, where recruitment is predominated by allosteric Ras binding. With this approach, we dissected the

role of allosteric regulation in SOS activation state transitions. Reconstitution of the activation of autoinhibited SOS^{HDPC} construct revealed two distinct activities of SOS: a transient activity and a burst-like activity. The transient activity was determined to be the result of short dwelling molecules that turnover one or few Ras molecules, whereas the burst activation was shown to be the result of long-dwelling single molecules of SOS that transitioned from fully autoinhibited to a highly active processive state. We demonstrated that both activities in SOS are sensitive to the density of Ras-GTP and, consequently, engage allosteric Ras. Thus, allosteric Ras binding is necessary, but not sufficient to access the highly active processive states in SOS. This suggests that a structural conformation unique to membrane-anchored SOS exists and potentially defines this hyperactive processive state. We anticipate that future structural studies will potentially resolve a membrane-specific structure of SOS that is distinct from the active conformation structures that have been identified in solution.

The reconstitution platform was extended to study the receptor-independent recruitment and activation of the full-length SOS protein. We observed that, contrary to SOS^{HDPC}, the transient activity is largely suppressed in SOS^{FL} and is insensitive to the density of Ras-GTP on membranes. This is consistent with work reporting that the C-terminal domain of SOS obstructs engagement of allosteric Ras(*15*). In the context of cellular signaling, spurious and unchecked activation from transient activity could have devastating consequences for cells. Our result reinforces the dual-regulatory role of the C-terminal domain of SOS(*29*), where it negatively regulates activity by contributing to enzyme autoinhibition and positively regulates activity by enabling Grb2-mediated membrane docking in response to the activation of receptors.

Despite the lack of transient activity, SOS^{FL} displayed bursts in Ras activation. The fact that the processive activity is the dominant activity observed in the full-length protein suggests that this is the main signaling competent state of SOS and is potentially present in the cellular context. Furthermore, we showed that the probability of SOS transitioning to this highly processive states increases with Ras-GTP density. This suggests an alternate pathway to establish positive feedback in Ras signaling, where Ras-GTP allosterically activates SOS by increasing the probability of SOS transitioning to a highly active processive state capable of overcoming negative pressure from GAPs and driving downstream signaling.

More fundamentally, our strategy shows how reconstitution approaches with simultaneous access to single molecule enzyme kinetics and activation readouts can be used to provide mechanistic insights. This approach is generalizable to a broad class of membrane-mediated reactions where release of enzyme autoinhibition at the membrane and allosteric activation are key determinants of signaling dynamics.

Chapter 4

Total reconstitution of receptor-mediated SOS activation *in vitro*

Adapted with permission from Huang, W. Y. C., Alvarez, S., Kondo, Y., Lee, Y. K., Chung, J.K. , Lam, H.Y.M., Biswas, K.H., Kuriyan, J., Groves, J.T. "A molecular assembly phase transition and kinetic proofreading modulate Ras activation by SOS", Science, 363**,** 1098–1103 (2019). Copyright 2019 Science.

4.1 Abstract

The guanine nucleotide exchange factor (GEF) Son of Sevenless (SOS) is a key Ras activator that is autoinhibited in the cytosol and activates upon membrane recruitment. Autoinhibition release involves structural rearrangements of the protein at the membrane and thus introduces a delay between initial recruitment and activation. In this study, we designed a single-molecule assay to resolve the time between initial receptor-mediated membrane recruitment and the initiation of GEF activity of individual SOS molecules on microarrays of Ras-functionalized supported membranes. The rise-and-fall shape of the measured SOS activation time distribution and the long mean time scale to activation (~50 seconds) establish a basis for kinetic proofreading in the receptor-mediated activation of Ras. We further demonstrate that this kinetic proofreading is modulated by the LAT (linker for activation of T cells)–Grb2–SOS phosphotyrosine-driven phase transition at the membrane.

4.2 Introduction

A key step in the mitogen-activated protein kinase (MAPK) pathway is the activation of the membrane-anchored Ras guanosine triphosphatase (GTPase) by guanine nucleotide exchange factors (GEFs), including Son of Sevenless (SOS)(*12*, *13*, *19*, *69*, *70*) . SOS, which is an important Ras GEF in T cell receptor (TCR) and epidermal growth factor receptor (EGFR) signaling, is recruited via Grb2 to activated receptors or scaffold proteins on the membrane, where it subsequently activates Ras(*12*). The influence of SOS dynamics in MAPK signaling is underscored by the relatively low SOS protein copy number in the EGFR-MAPK pathway(*71*). In addition to its GEF activity, SOS serves as a cross-linking molecule that, by interacting with two Grb2 molecules, forms linkages between receptor or scaffold

molecules(*36*, *37*). In the case of the scaffold protein linker for activation of T cells (LAT), multivalency of the phosphorylated tyrosine (pY) sites on LAT, which serve as Grb2 binding sites, enables the networked assembly of LAT-Grb2-SOS into a condensed two-dimensional gel or liquid phase on the membrane surface(*72*–*76*). Although similar protein assembly–mediated phase transitions are emerging as a general theme in several different signaling systems(*77*, *78*), little is known about how they regulate signaling.

We performed a detailed analysis of the molecular mechanism by which SOS autoinhibition is released after receptor-mediated recruitment to the membrane. We reconstituted purified full-length SOS (SOS^{FL}) along with Grb2 on supported membranes containing phosphorylated LAT and Ras to mimic the signaling geometry of the inner leaflet of the T cell plasma membrane. By developing a single-molecule activation assay in a membrane microarray format(*28*, *59*), we resolved the timing process from the initial membrane association to the initiation of GEF activity for each individual SOS molecule. The results reveal a long mean time delay (~50 s) between initial recruitment and the activation of SOS GEF activity. Additionally, the delay time distribution— exhibiting the distinctive rise and fall of a gamma distribution—reveals the existence of rate-limiting kinetic intermediates in the activation of SOS. These features of SOS autoinhibition release, along with the system's being intrinsically out of equilibrium, provide the basic requirements for a kinetic proofreading mechanism(*79*) in the activation of Ras(*73*). In such a mechanism, short-dwelling SOS molecules at the membrane may fail to achieve release of autoinhibition and thus fail to activate any Ras, whereas long-dwelling SOS molecules would exhibit disproportionately higher probabilities of activation. Such a screening process may be especially important for SOS because, once activated, SOS remains trapped at the membrane, where it can processively activate hundreds of Ras molecules (*15*, *28*, *29*).

Lastly, we experimentally demonstrate that the LAT-Grb2-SOS pY-mediated phase transition, which has been shown to extend SOS dwell times(*73*), strongly modulates the amount of Ras activated by a group of SOS molecules. These observations suggest a mechanism by which protein assembly phase transitions, such as LAT-Grb2SOS, modulate downstream signaling activity via kinetic discrimination or proofreading processes.

4.3 Reconstitution of receptor-mediated SOS activation with single-molecule resolution

Receptor-mediated activation of SOS is tightly regulated(*1*, *12*–*14*, *22*, *23*, *29*, *73*). The catalytic core of SOS, consisting of the Ras exchanger motif and a CDC25 domain, is flanked by a C-terminal proline-rich (PR) domain and N-terminal auto- inhibitory domains consisting of the histone fold, Dbl homology, and Pleckstrin homology domains (Fig. 4.1A). Mutations in the N-terminal domains of SOS can lead to the dysregulation of autoinhibition and the development of Noonan syndrome disorder(*80*). The PR domain binds the Src

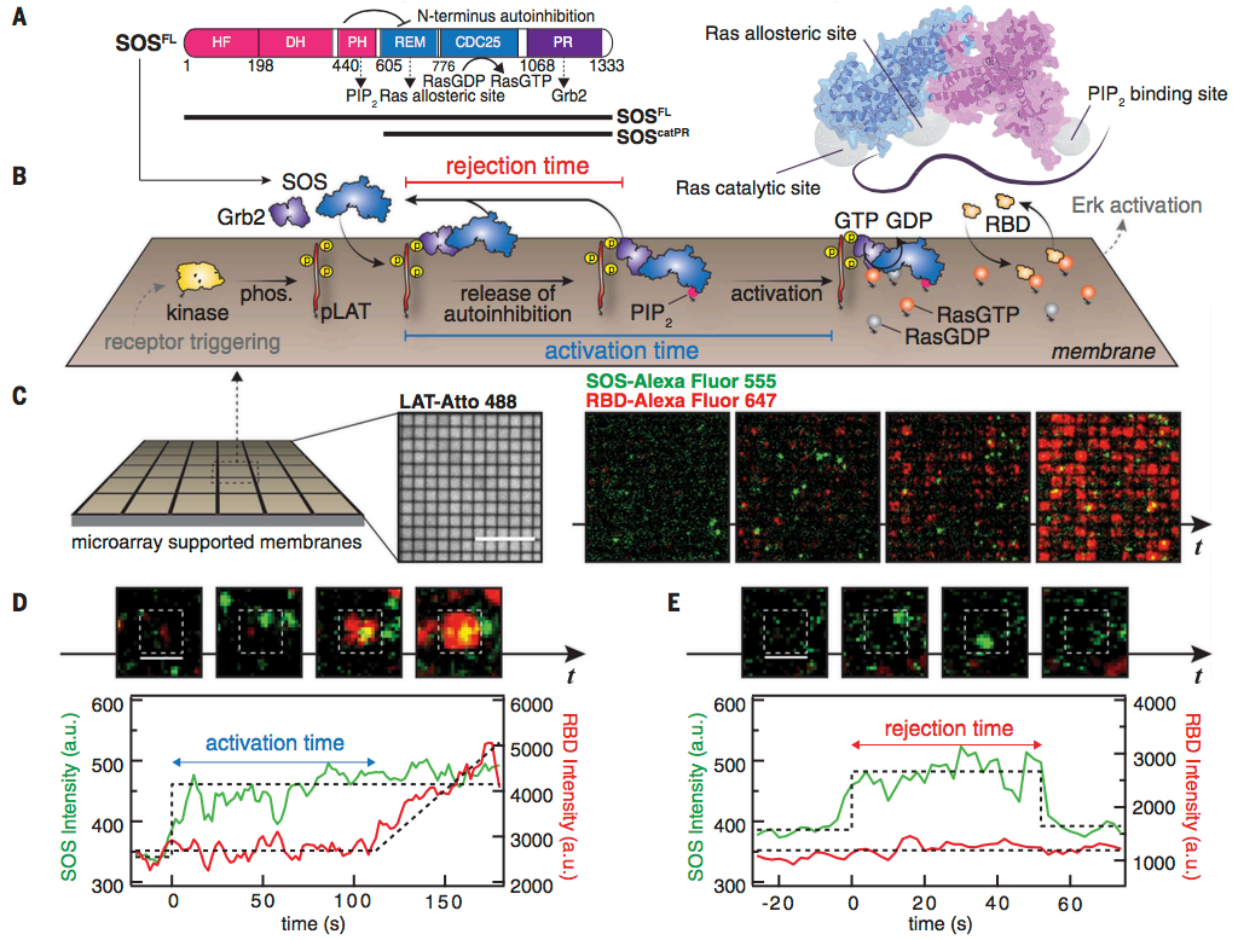

Fig. 4.1| Single-molecule activation assay of SOS^{FL} on supported membranes. (**A**) Domain architecture (left) and a cartoon model (right) of SOSFL. The crystal structure was rendered with Protein Data Bank entry 3KSY. HF, histone fold; DH, Dbl homology domain; PH, Pleckstrin homology domain; REM, Ras exchanger motif. Numbers indicate amino acid positions. (**B**) Schematic of the reconstitution of Grb2-mediated SOS activation. LAT phosphorylated by membrane-bound kinase Hck (pLAT) and Ras preloaded with GDP were decorated on the supported membranes corralled by 1-μm by 1-μm or 2-μm by 2-μm chromium grids. The injection of Grb2, SOSFL-Alexa Flour 555, RBD-K65E–Alexa Fluor 647, and GTP into the solution triggered SOS recruitment, subsequent release of autoinhibition, and activation. Receptor triggering and downstream activation (in gray) are shown to illustrate the signaling pathway, and not included in the experiments. phos., phosphorylation. (**C**) Snapshot images of SOS (green) and RBD (red) recruitment in microarray supported membranes. Scale bar, 10 mm. t, time. (**D**) Definition of activation time. (**E**) Definition of rejection time. [(**D**) and (**E**)] Scale bars, 2 μm. a.u., arbitrary units.

homology 3 (SH3) domains of Grb2, whereas the SH2 domain of Grb2 interacts with pY residues on membrane receptors such as LAT or EGFR, thereby localizing SOS onto membrane surfaces in response to receptor activation(*19*, *81*). Upon membrane recruitment, interactions of the SOS N-terminal domains with anionic lipids, such as phosphatidylinositol 4,5-bisphosphate (PIP2), facilitate the release of autoinhibition(*14*, *33*). The catalytic domains of SOS contain two binding sites for Ras: catalytic and allosteric(*24*). With Ras

engaged in the allosteric site, SOS remains on membranes for extended periods of time (>1 min) and enters a highly processive mode in which it catalyzes hundreds of Ras guanosine triphosphate (GTP)–loading events (*15*, *28*, *29*). Although there is growing understanding that a multitude of molecular interactions are critical for efficient SOS activation on membranes(*12*), real-time monitoring of receptor- mediated SOS activation has been inaccessible, in part because of challenges in SOS purification and the development of a membrane assay capable of resolving such features.

We developed a single-molecule activation assay on supported membranes to resolve the timing of SOS activation from membrane recruitment to the initiation of nucleotide turnover in Ras (Fig. 4.1B). Supported membranes consisting primarily of DOPC (1,2-dioleoyl-sn-glycero-3-phosphocholine) lipids doped with 2% PIP2, 2% MCC-DOPE {1,2-dioleoyl-sn-glycero-3-phosphoethanolamine-N-[4-(p-maleimidomethyl)cyclohexane-carboxamide]}, and 4% Ni2+–NTA-DOGS {1,2-dioleoyl-sn-glycero- 3-[(N-(5-amino-1-carboxypentyl) iminodiacetic acid) succinyl]} were deposited on a glass substrate by vesicle fusion. Cytoplasmic domains of the Src kinase Hck and the adaptor protein LAT, both with six-histidine (His_6) tags, were tethered to the supported membrane through His_6 interactions with nickel-chelating lipids (*82*). Although Hck is not an efficient kinase for the phosphorylation of LAT(*83*), it phosphorylates LAT to completion, given sufficient time. H-Ras molecules were covalently attached to membranes via maleimide chemistry with the MCC-DOPE lipids(*84*). All of these proteins reconstituted on supported membranes were laterally mobile, with typical densities of <100, ~800, and ~500 μm^{-2} for Hck, LAT, and Ras, respectively. The LAT densities in the reconstitution are comparable to those measured in cells(*85*). Although Ras local densities in cells can vary widely, we used densities similar to those of Ras clusters (>1000 μm^{-2}) in cells(*51*, *86*). LAT was fully phosphorylated by Hck before the addition of SOS, as monitored by the recruitment of fluorescent Grb2(*73*). SOS^{FL} was prepared by intein ligation(*87*) of the N-terminal flanked catalytic domain and the C-terminal PR domain of human SOS1. By adding ~1 nM SOS^{FL} and 20 nM Grb2 in solution [the concentrations are comparable to recent quantifications of protein abundance in the EGFR-MAPK pathway(*71*); dissociation constant Kd ~ 10 μM(*88*), single-molecule membrane recruitment of SOS via Grb2 can be clearly resolved by total internal reflection fluorescence (TIRF) microscopy. If Grb2 was not included, we observed ~90% lower SOS recruitment. On membranes, SOS catalyzes the nucleotide exchange of Ras [preloaded with guanosine diphosphate (GDP)] with GTP in solution. Ras-GTP levels are read out via the rapidly reversible binding of a fluorescently labeled Ras-binding domain (RBD) (40 nM in solution). The RBD used in this study is a mutant [Lys65→Glu (K65E)] derived from Raf-1; it has faster binding kinetics than the wild-type RBD(*58*) providing real-time (~1-s) Ras-GTP density measurements to precisely identify the moment of SOS activation.

We resolve the activity of single SOS^{FL} molecule recruitment events by localizing the reactions into small corrals separating patches of fluid membranes(*28*) (Fig. 4.1C). This strategy allows precise assignment of the amount and timing of Ras activation to individual

SOS recruitment events. In practice, this was achieved by corralling the supported membranes with 1-μm by 1-μm or 2-μm by 2-μm grid arrays of chemically inert chromium barriers, which are pre-fabricated onto the underlying substrate before membrane deposition(*59*). The chromium barriers are typically ~10 nm in height, and although they are effective barriers to the mixing of membrane- associated components, they pose essentially no barrier to the flow of molecules in the adjoining solution. Both LAT and Ras showed small variations (<10%) across different arrays. This membrane microarray strategy also facilitates simultaneous sampling of large numbers (~1000) of nearly identical membrane corrals, all in contact with the same solution.

The simultaneous imaging of SOS^{FL}–Alexa Fluor 555 and RBD-K65E–Alexa Fluor 647 at a frame rate of 0.5 Hz recorded when and where SOS recruitment and activation occurred (Fig. 4.1, C to E). Once activated, SOS processively catalyzes nucleotide exchange in Ras at a relatively rapid rate, providing a distinctly discernable transition between inactive and active states of SOS (see fluorescence intensity traces in Fig. 4.1D). Additionally, SOS tends to stay active for an extended period of time(*15*, *28*). Specifically, we parsed out corrals with a single SOS recruitment event and then measured the time to the onset of RBD recruitment, indicating the activation of SOS. The SOS recruitment-activation trajectories can be classified into two types: recruitment of SOS followed by activation (Fig. 4.1D) and recruitment and dissociation of SOS without activation (Fig. 4.1E). The first type of trajectory reveals the time interval between initial membrane engagement and the release of SOS autoinhibition, enabling GEF activity, which we define as the activation time. The latter trajectory indicates the membrane dwell times for SOS molecules that unbind from the membrane before activating, which we define as the rejection time. The shape of the activation time distribution is especially informative. The existence of rate-limiting intermediates, through which SOS must pass en route to activation, will create a distinctive rise-and-fall shape (gamma distribution), whereas an exponential activation time distribution will indicate that autoinhibition release follows a first-order process. The implication of this kinetic detail is that kinetic proofreading mechanisms, under which long-dwelling molecules are disproportionately more likely to activate, can operate only in the first case, with rate-limiting kinetic intermediates(*73*, *79*).

A single SOS recruitment event results in either activation or rejection. By collecting ensembles of these single-molecule recruitment-activation trajectories, we compiled histograms of the activation and rejection time distributions, which also reveal the relative probabilities of these two outcomes (Fig. 4.2, A and B). The activation time distribution exhibits the rise-and-fall shape of a gamma distribution, with a rather long mean delay of 55 s and a standard deviation of 44 s (Fig. 2A). The time resolution of detectable activation in the current experiment is <2 s, evident because RBD-K56E binding to Ras-GTP has fast binding kinetics (dwell time, ~100 ms) and some trajectories show rapid RBD recruitment (<2 s) after SOS binding to membranes. The rejection time distribution is roughly

exponential in shape, with a mean of 30 s and a standard deviation of 29 s (Fig. 4.2B). The shapes of these distributions reveal underlying mechanistic features of SOS regulation.

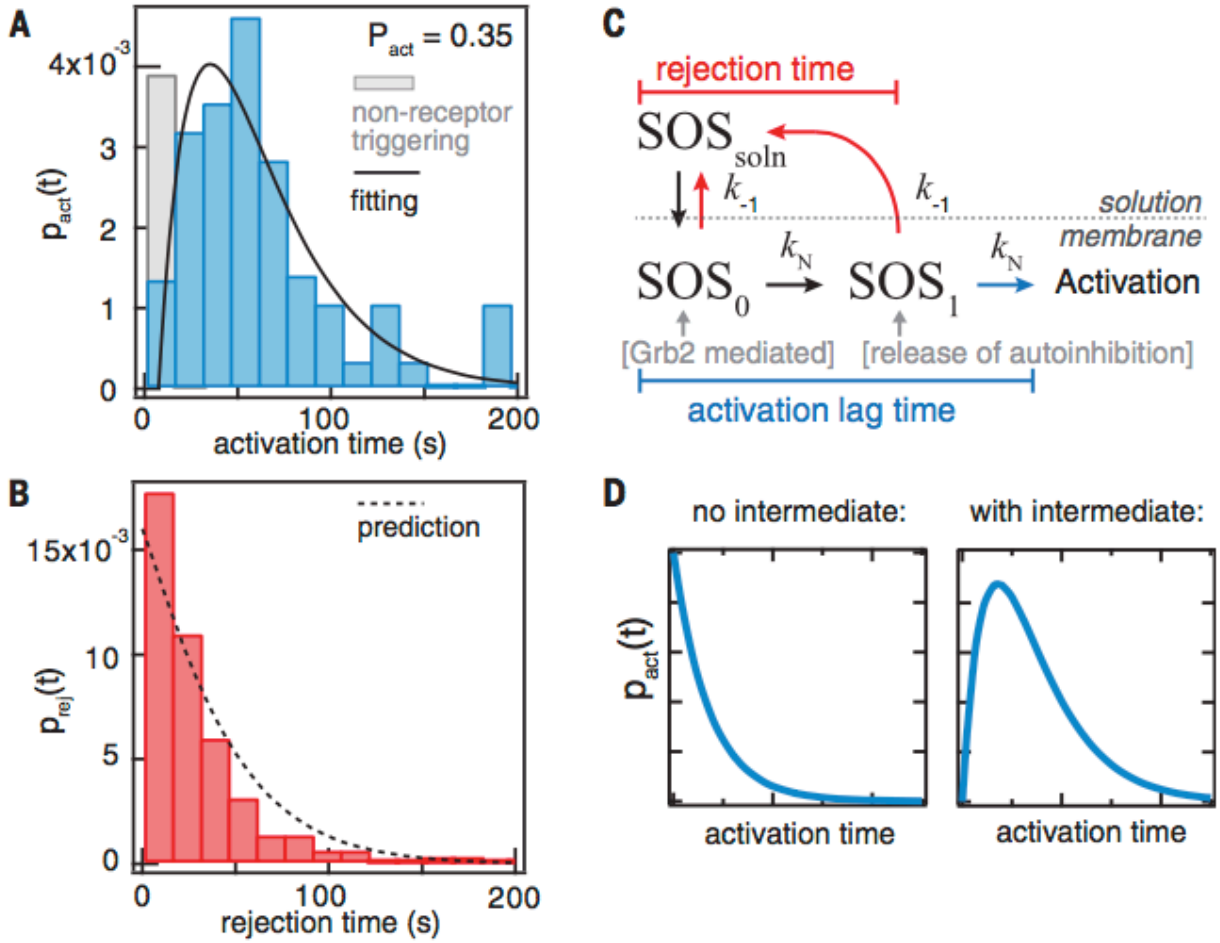

Fig. 4.2| Activation time distribution of SOS. (**A** and **B**) Histograms of the activation time and rejection time of Grb2-mediated SOSFL recruitment from the single-molecule activation assay. The solid line is fitting to the model in (**C**); the fitted values are k_N = 0.02 s^{-1} and -1 = 0.016 s^{-1}. The dashed line represents the prediction by the model using fitted values from the activation time distribution. (**C**) A simple model of SOS^{FL} activation. k_N denotes the transition rate constants for the kinetic intermediates, and k_{-1} represents the dissociation rate constants from membranes. SOS_{soln}, SOS in solution. (**D**) Without a kinetic intermediate (N = 0), the activation time distribution is an exponential distribution peaked at t = 0. In contrast, the existence of at least one intermediate produces the characteristic rise-and-decay shape for the activation time distribution.

To quantitatively analyze these measured probability distributions, we construct a simple kinetic model in which the activation of SOS on membranes is described by the competing kinetics between activation and dissociation from membrane surfaces (Fig. 4.2C) (for derivations, see Appendix B.2) (*73*, *89*, *90*). In this model, SOS binds to membranes initially in an autoinhibition state (SOS_0), and the release of autoinhibition is achieved after overcoming a series of kinetic intermediates. Alternatively, SOS may unbind from the

membrane, going back into solution, where it eventually relaxes back to its native autoinhibited state (SOS_0). Given N number of kinetic intermediate(s) in the activation pathway, the activation time distribution has the form

$$p_{act}(t) = p_N(t) \cdot e^{-k_{-1}t}$$

where p_N is the activation time distribution for a linear multistep process, arising from the convolution of (N + 1) single Poisson steps with rate constants k_i, and k_{-1} is the dissociation rate constant. The overall probability of SOS activation, P_{act} ,depends on both the transition rate (k_i) and the unbinding rate (k_{-1}) and is given by $P_{act} = \int_0^\infty p_{act}(t)\, dt$. A similar expression defines the overall probability of rejection, P_{rej} , in terms of the rejection time distribution, p_{rej} and the integrated sum of these two distributions normalizes to one.

In a case with a single rate-limiting step or multiple steps with similar rates, $p_N(t)$ approaches a gamma distribution, $p_N(t) = k_N^{N+1} t^N e^{-k_N t}/N!$. This approximation provides a useful intuition about the shape of the activation time distribution: The existence of intermediate(s) predicts a rise-and-fall shape to the distribution (Fig. 4.2D). In the alternative case, without any kinetic intermediates (N = 0), the activation time distribution is strictly exponential (Fig. 4.2D). The observed data (Fig. 4.2A) are consistent with the first case, indicating that SOS activation on membranes involves progressing through at least one rate- limiting kinetic intermediate, with a low transition rate (k_N) of 0.02 s^{-1}. In practice, the kinetic observation will be dominated by the slowest kinetic step for a unidirectional activation mechanism(*29*). Thus, we used N = 1 to analyze the distributions, i.e.,$p_{act}(t) = k_N^2 t e^{-(k_N + k_{-1})t}$. If this model is sufficient to describe SOS activation, the fitted values from the activation time distribution should, with no additional fit parameters, predict the rejection time distribution (Fig. 4.2B), which is given by

$$p_{rej}(t) = \frac{\Gamma(N, T)}{N!} \cdot k_{-1} e^{-k_{-1}t}$$

where $\Gamma(N, T) = \int_{k_N t}^\infty t'^N e^{-t} dt$ the upper incomplete gamma function. In the case of N= 1, $p_{rej}(t) = k_{-1}(k_N t + 1) e^{-(k_N + k_{-1})t}$. The experimentally measured rejection time distribution is well described by the prediction based on parameters measured from the activation time distribution (Fig. 4.2B). The activation time distribution of SOS is indicative of an activation mechanism dominated by a single rate-limiting kinetic intermediate. This model does not exhaust all possible routes of activation but delineates the main pathway. In addition, it is possible that SOS dissociation from membranes is a multistep process, but it is likely much faster than the activation time scale such that the data are well described by the simple model.

4.4 Regulation of autoinhibition defines activation timing of SOS and kinetic proofreading capability

The activation time of SOS is determined, in part, by the release of autoinhibition of the catalytic domains by the N-terminal domains. We compared Grb2-mediated SOS recruitment

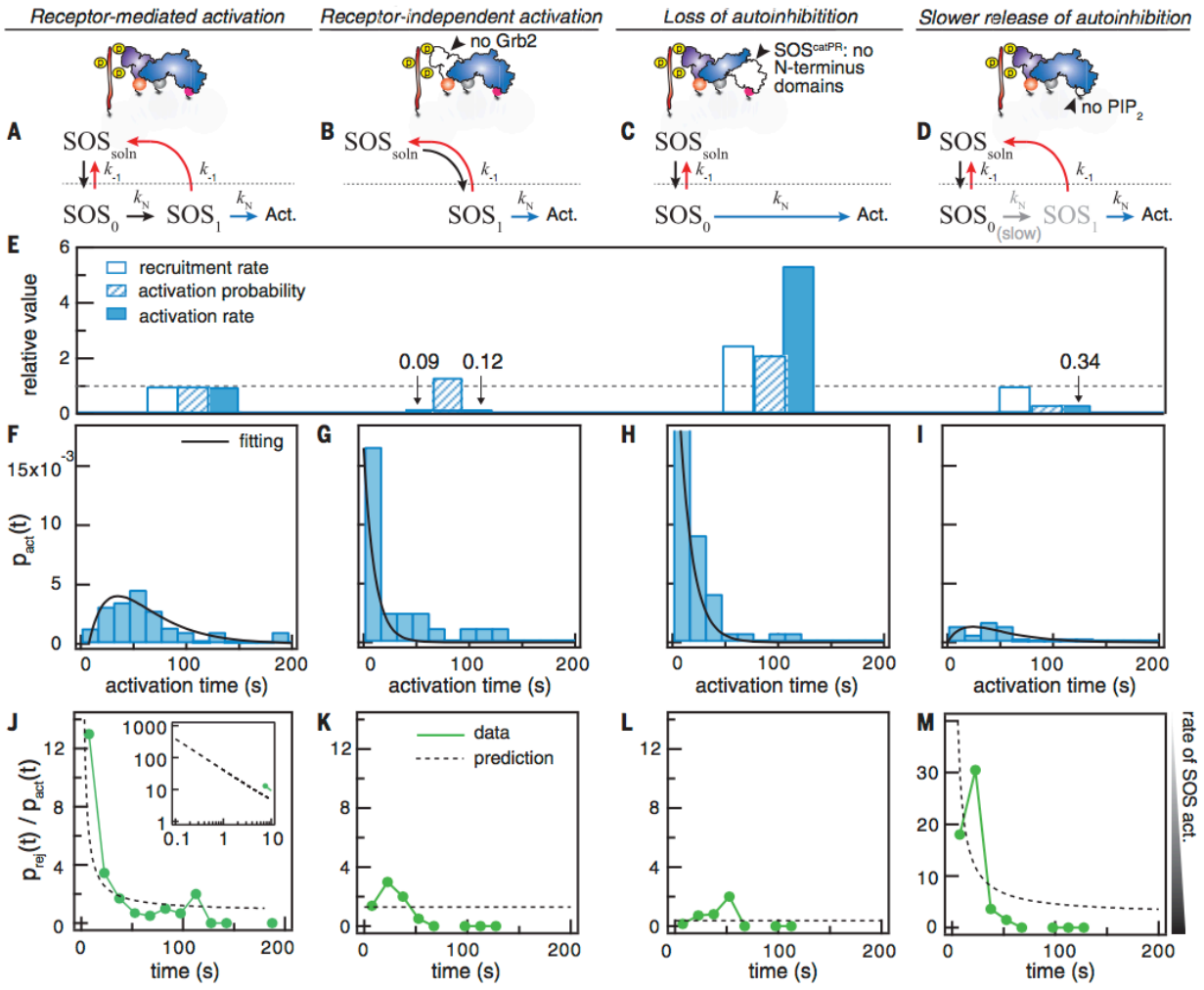

Fig. 4.3| The regulation of autoinhibition defines the activation timing of SOS and its kinetic proofreading capability. The top schematics show the experimental design (**A** to **D**) The kinetic models for Grb2-mediated SOS^{FL} activation, SOS^{FL} activation without Grb2, SOS^{catPR} activation, and SOS^{FL} activation without PIP2. Act., activation. (**E**) The relative recruitment rate, activation probability, and activation rate for each condition. Activation rate = recruitment rate x activation probability. The Grb2-mediated recruitment rate of SOS^{FL} was 3×10^{-3} s^{-1} μm^{-2}. The dashed line is at 1. (**F** to **I**) The activation time distribution for each condition. Black lines are fitting to the models in (**A**) to (**D**). (**F**) is the same data from Fig. 2a. (**J** to **M**) The ratio between rejection and activation counts as a function of SOS dwell time. The inset in (**J**) shows the model's extrapolation for very short dwelling SOS. Dashed lines are predictions by the models in (**A**) to (**D**).

and activation with three other orthogonal activation profiles (Fig. 4.3): (i) receptor-independent activation without Grb2 (Fig. 4.3B), (ii) activation without N-terminal autoinhibition using the construct SOS^{catPR} (Figs. 4.1A and 4.3C), and (iii) hindered activation without PIP2 (Fig. 4.3D). Although the recruitment rate of SOS is markedly enhanced by Grb2 (Fig. 4.3E), these three cases exhibit fundamental differences in the activation time compared with Grb2-dependent activation (Fig. 4.3, F to I). Cases (i) and (ii) result in single-step activation (i.e., the activation time distribution is exponentially shaped) over the experimental time scale of 1 to 200 s. Without Grb2, spontaneous activation of SOS^{FL} is (rarely) observed as a result of SOS apparently fluctuating into an active configuration before interacting with the membrane. In this state, SOS^{FL} binds to Ras directly and begins to processively activate Ras without the need to pass through the kinetic intermediate. This detail is revealed by the exponential shape of the activation time distribution for these spontaneous activation events. Before successful purification of SOS^{FL}, these are the only activation events that have been observed in prior studies(*28*, *29*). The SOS^{catPR} construct lacks N-terminal autoinhibition and also apparently lacks the kinetic intermediate, as revealed by its exponentially shaped distribution (Fig. 4.3, G and H). Case (iii), lacking PIP2 in the membrane, exemplifies the scenario where the activation pathway on the membrane is hindered, as revealed by a decreased activation rate, yet the kinetic bottleneck is retained, as revealed by the rise-and-fall shape of the activation time distribution (Fig. 4.3I).

Together, these data provide a molecular description of the autoinhibition release process of SOS^{FL}: The first recruited state (SOS_0) corresponds to Grb2-mediated recruitment while under the protection of autoinhibition. The slowest intermediate (SOS_1) involves PIP2-mediated re- lease of autoinhibition (Figs. 2C and 3, A to D). Finally, fully activated SOS presumably involves locking Ras into the allosteric pocket(*22*, *28*), enabling the processive catalysis.

A multistep activation process, such as we have observed for SOS^{FL}, can, in principle, lead to longer-dwelling molecules having disproportionally higher activation rates(*73*) —this is classically known as kinetic proofreading(*79*). To test for this behavior experimentally, we examined the ratio p_{rej}/p_{act} as a function of SOS dwell time from the corral experiments. This analysis compares the rate (probability per unit of time) of SOS activation for different dwell times (Fig. 4.3, J to M). The kinetic intermediate defined by autoinhibition release greatly enhances the proofreading capability, as evident from the decaying functional form of the $p_{rej}(t)/p_{act}(t)$ curve for SOS^{FL} (Fig. 4.3, J and M). By contrast, a weakly discriminating process will have a near-constant curve, as observed for SOS^{catPR} molecules lacking kinetic intermediates (Fig. 4.3, K and L). These data provide evidence that SOS^{FL} activity is capable of being modulated by a kinetic proofreading mechanism.

With a proofreading mechanism at play, the rate of Ras activation depends disproportionately on the membrane dwell times of SOS. Given that the individual pY-Grb2

interactions exhibit fast kinetics [mean dwell time, ~0.1 s(*73*)] compared with the mean activation time of SOS measured in this study (~55 s), we speculate that monovalent recruitment of SOS to the mem- brane by Grb2 is unlikely to lead to Ras activation. However, SOS dwell time on the membrane can be greatly elongated when SOS interacts with more than one Grb2 molecule. Single-molecule tracking of SOS shows that the initial stable recruitment of SOS (dwell time > 1 s) is mediated primarily by Grb2 instead of PIP2 or Ras. Furthermore, mobility analysis indicates that stably recruited SOS is interacting with at least two LAT molecules via multiple Grb2 molecules.

4.5 Molecular assembly enhances Ras activation by SOS

Recent studies have vividly demonstrated that LAT-Grb2-SOS can undergo a phase transition to form a condensed two-dimensional liquid or gel state consisting of a networked molecular assembly on the membrane surface(*72*–*76*). A distinctive feature of these condensed phases is that multivalent interaction of SOS within the network can markedly elongate SOS dwell time on the membrane(*73*). To explore the effect of this protein assembly network on Ras activation, we added the PR domain of SOS, which has no intrinsic catalytic activity but allows formation of the assembly, into the corral experiments (Fig. 4.4, A and B). If the PR domain acted solely as a competitor, titrating it would decrease Ras activation by outcompeting the fixed concentration of SOS^{FL}. Instead, we observed that the rate of Ras activation increased substantially when the PR domain was added (50 nM) (Fig. 4.4, C to E), suggesting that LAT assemblies promote Ras activation. Notably, this enhanced activation by the PR domain was absent at low LAT densities, where assemblies cannot form; titrating the PR domains to a higher concentration (≥100 nM in our experiments) also abolished this enhancement by outcompeting SOS^{FL}. Furthermore, the two-fold increase in SOS^{FL} recruitment with the PR domain is insufficient to explain the eightfold increase in Ras activation (Fig. 4.4, C to E).

To quantitatively account for the effect of Grb2-mediated SOS dwell time at the membrane on the probability of SOS activation, we first evaluated the activation probability of SOS per recruitment event, $P_{act} = \int_0^\infty p_{act}(t)\, dt$. P_{act} is intrinsically a function of the Grb2-mediated SOS dwell time, as longer-dwelling SOS molecules have a higher likelihood of activation before unbinding. The functional dependence of P_{act} on the mean dwell time is plotted in Fig. 4F, on the basis of the measured activation time distribution of SOS (Fig. 4.2) (N = 1 intermediate). This calculation reveals that Pact is highly sensitive to the SOS dwell time when the mean activation time is substantially longer than the mean dwell time, which is the case in our reconstitution and likely in live cells as well(*77*). Next, we evaluated the fold increase in SOS activity per molecule, x_{SOS} (the definition is provided in materials and methods), as a function of change in the mean dwell time. Figure 4.4F enables a direct comparison of SOS activation probabilities in the unassembled and assembled LAT configurations in Fig. 4.4, D and E. Single-molecule analysis reveals that the fraction of long-dwelling species of SOS increases with the addition of the PR domain (and con- sequent LAT

assembly) in this experiment, although the degree of molecular assembly is not as large as that observed in a fully condensed phase(*73*). The roughly fourfold net increase in Ras activation per SOS molecule (after accounting for recruitment) is comparable to the estimation on the basis of mean dwell time changes (from ~4 to 6 s). Thus, relatively small changes in the SOS dwell time lead to large changes in the probability of activation because the system is operating under conditions in which the overall probability of activation is low

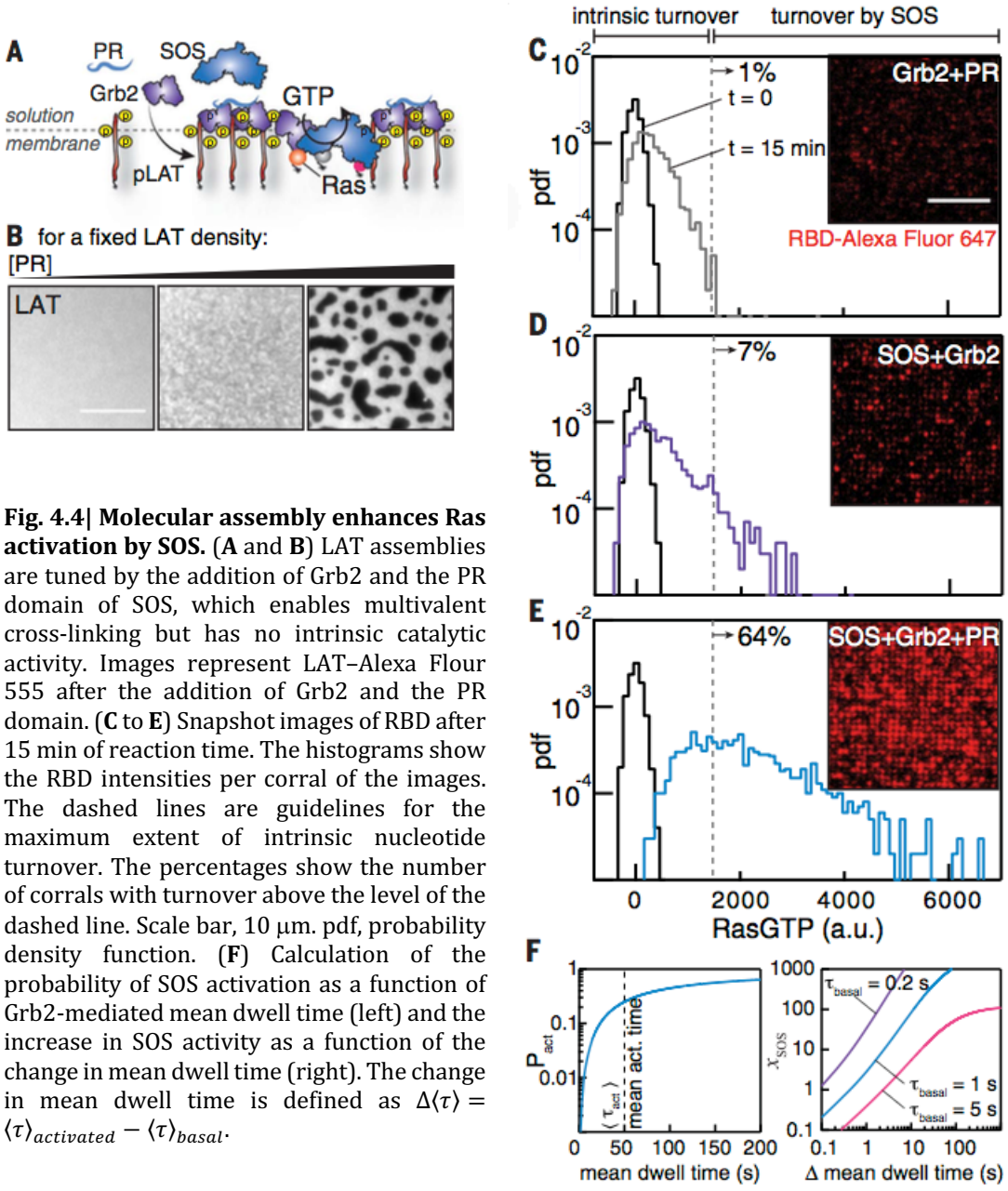

Fig. 4.4| Molecular assembly enhances Ras activation by SOS. (**A** and **B**) LAT assemblies are tuned by the addition of Grb2 and the PR domain of SOS, which enables multivalent cross-linking but has no intrinsic catalytic activity. Images represent LAT–Alexa Flour 555 after the addition of Grb2 and the PR domain. (**C** to **E**) Snapshot images of RBD after 15 min of reaction time. The histograms show the RBD intensities per corral of the images. The dashed lines are guidelines for the maximum extent of intrinsic nucleotide turnover. The percentages show the number of corrals with turnover above the level of the dashed line. Scale bar, 10 μm. pdf, probability density function. (**F**) Calculation of the probability of SOS activation as a function of Grb2-mediated mean dwell time (left) and the increase in SOS activity as a function of the change in mean dwell time (right). The change in mean dwell time is defined as $\Delta\langle\tau\rangle = \langle\tau\rangle_{activated} - \langle\tau\rangle_{basal}$.

(e.g., the mean dwell time is substantially shorter than the mean activation time). Monovalent recruitment interactions between SOS and phosphorylated LAT via Grb2 are brief (<1 s) (*73*) and will thus have an exceptionally low probability of successful SOS activation. In the fully condensed state, the LAT- Grb2-SOS assembly can elongate SOS dwell times by more than an order of magnitude(*73*), which is even more than that achieved in the PR domain experiments presented here. Collectively, these data suggest that LAT-Grb2-SOS assembly can exert a powerful influence over SOS activation by modulating the SOS dwell time at the membrane.

In resting T cells, LAT typically exhibits some basal level of phosphorylation (*91*). A proofreading mechanism in SOS activation can prevent the spontaneous membrane localization of SOS from activating Ras and thus prevent upstream basal pY activity from activating certain downstream pathways. This kinetic proofreading at the level of SOS is different from kinetic proof- reading at the TCR, which has been proposed to contribute to antigen discrimination on the basis of peptide major histocompatibility complex– TCR binding kinetics (*92*).

The type of kinetic proofreading identified here in the activation of Ras by SOS reveals a potentially broad mechanism by which membrane recruitment kinetics can be used to modulate downstream signaling activity. Many membrane- associated signaling molecules activate in a multi- step fashion—for example, Vav (GEF for Rho family GTPase)(*93*), Raf (*94*), class I protein kinase C-α(*95*), phosphoinositide 3-kinases(*96*), and inducible T cell kinase. The initiation of actin nucleation by the Arp2/3 complex is also a slow multistep process. Notably, the actin regulator neuron Wiskott-Aldrich syndrome protein (N- WASP) and the Arp2/3 complex have recently been shown to exhibit dwell time–dependent activity modulation by nephrin–Nck–N-WASP condensation phase transition, in a mechanism highly parallel to that described here for Ras and SOS(*78*, *97*). Hence, we speculate that the timing and proofreading mechanism observed in this study is not exclusive to SOS but is a common theme in signal regulation at the membrane.

Chapter 5

Conclusions and outlook

5.1 Final Remarks

The work presented in this dissertation extends the technologies for the reconstitution of Ras on membranes and applies them to interrogate otherwise inaccessible features and mechanisms of the signaling pathway. Key results include:

- The development of an *in vitro* platform with a real-time, selective, and fully reversible readout of Ras activation on supported membranes. The engineering of an RBD-based sensor extends the Ras supported membrane platform by enabling the monitoring the dynamic switch cycling of Ras. (Chapter 2)

- The RBD of Raf1 has an underappreciated tendency to oligomerize upon binding membrane coupled Ras. This tendency was removed by N-terminal tagging of RBD. (Chapter 2)

- Allosteric Ras binding in SOS is necessary but not sufficient to determine access to highly active processive states. These states potentially correspond to a distinct structural conformation of SOS at the membrane that is yet to be identified. (Chapter 3)

- Allosteric activation by Ras-GTP increases the probability of SOS transitioning to highly active processive states, suggestive of an alternate mechanism behind positive feedback in Ras signaling. (Chapter 3)

- The multiple layers of regulation in SOS activation, from Grb2-mediated membrane recruitment to release of autoinhibition, establish the basis for kinetic proofreading in Ras signaling. (Chapter 4)

- Kinetic proofreading in SOS activation is modulated by the phosphotyrosine-driven phase transition of LAT (Chapter 4)

The findings presented in this dissertation aim to further our understanding of different aspects of the multilayered activation of SOS. This multistep process involving membrane

recruitment via Grb2, lipid binding, release of autoinhibition, and allosteric Ras binding, resulting in the activation of SOS(*12*). Active SOS remains anchored to the membrane by lipid interactions and allosteric Ras binding, processively turning over hundreds of Ras molecules until removed by endocytosis(*29*). The allosteric activation of SOS is modulated by Ras-GTP, introducing positive feedback and signal amplification in Ras signaling(*22*, *27*, *66*). In T-cells (*36*, *37*), and potentially in other cell systems, all these steps happen in the context of SOS-mediated protein assemblies at the membrane that are believed to regulate signaling from SOS.

The processive activity of SOS is a strong driver of Ras signal propagation and is a potential source of signal amplification in Ras signaling(*15*, *28*, *29*). The contribution of SOS processivity to positive feedback and signal amplification was explored in Chapter 3. To address this, we investigated the role of allosteric Ras binding in mediating SOS processive activity. Our observations showed that allosteric Ras binding is necessary, but not sufficient to fully determine SOS processive activity. Allosteric Ras binding was found to be a shared feature of a SOS-mediated activity distinct from SOS processivity. This suggests that, in addition to allosteric Ras binding, SOS processivity involves a distinct structural rearrangement at the membrane. Despite not fully determining the transition to SOS processive activity, allosteric binding of Ras-GTP was shown to increase the probability SOS processive activity. Altogether, these observations are suggestive of a positive feedback mechanism where allosteric activation of SOS enables access to highly active processive states, with the potential of amplifying and driving forward signal propagation from Ras.

In addition to the structural elements in SOS, cells have implemented other checkpoints in the Ras signal propagation. Chapter 4 of this dissertation investigates the role of SOS-mediated two-dimensional phase transitions in modulating Ras signal propagation. Reconstitution of the LAT, Grb2, and full-length SOS assembly process on Ras decorated membranes enabled dissecting recruitment and activation kinetics of single of single SOS enzymes. Quantification of the delay time between membrane recruitment and activation revealed that the receptor-mediated recruitment and release of autoinhibition introduces a threshold to the duration of a binding event to propagate downstream activation. The phase transition of LAT-Grb2-SOS was found to enhance Ras activation by increasing the probability of SOS molecules crossing the dwell time threshold. Collectively, the threshold in timing for SOS activation and modulation by phase transition introduces kinetic proofreading in Ras signaling pathway, where spurious activation from short SOS dwells are filtered out and propagation of true signals is ensured by the assembly processes.

From a technology perspective, this work contributes to the advancement of the Ras supported bilayer platform by expanding Ras activation readouts, introducing new membrane inputs, and implementing multichannel imaging strategies to dissect surface-mediated reactions. The engineering of the RBD as a reporter for Ras activation on supported membranes makes now possible the study of GAP catalyzed hydrolysis and GAP/GEF competition reactions (Chapter 2). Functionalization of Ras-decorated membranes with

scaffold proteins like LAT gives access to unique aspects in the regulation of Ras signaling, such as phosphotyrosine-driven recruitment of proteins to membranes and two-dimensional phase transitions (Chapter 4). Finally, the implementation of multichannel imaging strategies throughout these studies have enabled dissecting reaction kinetics by deconvolving enzyme recruitment and activity with high spatiotemporal resolution (Chapter 3 & 4).

Bibliography

1. J. T. Groves, J. Kuriyan, Molecular mechanisms in signal transduction at the membrane. *Nat. Struct. Mol. Biol.* **17**, 659–665 (2010).
2. S. D. Hansen *et al.*, Stochastic geometry sensing and polarization in a lipid kinase-phosphatase competitive reaction. *Proc. Natl. Acad. Sci. USA*. **116**, 15013–15022 (2019).
3. I. R. Vetter, A. Wittinghofer, The guanine nucleotide-binding switch in three dimensions. *Science*. **294**, 1299–1304 (2001).
4. A. E. Karnoub, R. A. Weinberg, Ras oncogenes: split personalities. *Nat. Rev. Mol. Cell Biol.* **9**, 517–531 (2008).
5. A. G. Stephen, D. Esposito, R. K. Bagni, F. McCormick, Dragging ras back in the ring. *Cancer Cell*. **25**, 272–281 (2014).
6. J. M. Ostrem, U. Peters, M. L. Sos, J. A. Wells, K. M. Shokat, K-Ras(G12C) inhibitors allosterically control GTP affinity and effector interactions. *Nature*. **503**, 548–551 (2013).
7. J. Canon *et al.*, The clinical KRAS(G12C) inhibitor AMG 510 drives anti-tumour immunity. *Nature*. **575**, 217–223 (2019).
8. J. Hallin *et al.*, The KRASG12C Inhibitor MRTX849 Provides Insight toward Therapeutic Susceptibility of KRAS-Mutant Cancers in Mouse Models and Patients. *Cancer Discov.* **10**, 54–71 (2020).
9. D. Bar-Sagi, E. H. Knelson, L. V. Sequist, A bright future for KRAS inhibitors. *Nat. Cancer*. **1**, 25–27 (2020).
10. J. L. Bos, H. Rehmann, A. Wittinghofer, GEFs and GAPs: critical elements in the control of small G proteins. *Cell*. **129**, 865–877 (2007).
11. C. Guerrero *et al.*, Expression of alternative forms of Ras exchange factors GRF and SOS1 in different human tissues and cell lines. *Oncogene*. **12**, 1097–1107 (1996).
12. P. Bandaru, Y. Kondo, J. Kuriyan, The Interdependent Activation of Son-of-Sevenless and Ras. *Cold Spring Harb. Perspect. Med.* **9** (2019), doi:10.1101/cshperspect.a031534.
13. H. Sondermann *et al.*, Structural analysis of autoinhibition in the Ras activator Son of sevenless. *Cell*. **119**, 393–405 (2004).
14. J. Gureasko *et al.*, Role of the histone domain in the autoinhibition and activation of the Ras activator Son of Sevenless. *Proc. Natl. Acad. Sci. USA*. **107**, 3430–3435 (2010).
15. Y. K. Lee *et al.*, Mechanism of SOS PR-domain autoinhibition revealed by single-molecule assays on native protein from lysate. *Nat. Commun.* **8**, 15061 (2017).

16. G. M. Findlay, T. Pawson, How is SOS activated? Let us count the ways. *Nat. Struct. Mol. Biol.* **15**, 538–540 (2008).
17. S. E. Egan *et al.*, Association of Sos Ras exchange protein with Grb2 is implicated in tyrosine kinase signal transduction and transformation. *Nature*. **363**, 45–51 (1993).
18. L. Buday, J. Downward, Epidermal growth factor regulates p21ras through the formation of a complex of receptor, Grb2 adapter protein, and Sos nucleotide exchange factor. *Cell*. **73**, 611–620 (1993).
19. N. W. Gale, S. Kaplan, E. J. Lowenstein, J. Schlessinger, D. Bar-Sagi, Grb2 mediates the EGF-dependent activation of guanine nucleotide exchange on Ras. *Nature*. **363**, 88–92 (1993).
20. P. Chardin *et al.*, Human Sos1: a guanine nucleotide exchange factor for Ras that binds to GRB2. *Science*. **260**, 1338–1343 (1993).
21. N. Li *et al.*, Guanine-nucleotide-releasing factor hSos1 binds to Grb2 and links receptor tyrosine kinases to Ras signalling. *Nature*. **363**, 85–88 (1993).
22. J. Gureasko *et al.*, Membrane-dependent signal integration by the Ras activator Son of sevenless. *Nat. Struct. Mol. Biol.* **15**, 452–461 (2008).
23. K. K. Yadav, D. Bar-Sagi, Allosteric gating of Son of sevenless activity by the histone domain. *Proc. Natl. Acad. Sci. USA*. **107**, 3436–3440 (2010).
24. S. M. Margarit *et al.*, Structural evidence for feedback activation by Ras.GTP of the Ras-specific nucleotide exchange factor SOS. *Cell*. **112**, 685–695 (2003).
25. S. Corbalan-Garcia, S. M. Margarit, D. Galron, S. S. Yang, D. Bar-Sagi, Regulation of Sos activity by intramolecular interactions. *Mol. Cell. Biol.* **18**, 880–886 (1998).
26. G. M. Findlay *et al.*, Interaction domains of Sos1/Grb2 are finely tuned for cooperative control of embryonic stem cell fate. *Cell*. **152**, 1008–1020 (2013).
27. J. Das *et al.*, Digital signaling and hysteresis characterize ras activation in lymphoid cells. *Cell*. **136**, 337–351 (2009).
28. L. Iversen *et al.*, Molecular kinetics. Ras activation by SOS: allosteric regulation by altered fluctuation dynamics. *Science*. **345**, 50–54 (2014).
29. S. M. Christensen *et al.*, One-way membrane trafficking of SOS in receptor-triggered Ras activation. *Nat. Struct. Mol. Biol.* **23**, 838–846 (2016).
30. C. A. Karlovich *et al.*, In vivo functional analysis of the Ras exchange factor son of sevenless. *Science*. **268**, 576–579 (1995).
31. L. McCollam *et al.*, Functional roles for the pleckstrin and Dbl homology regions in the Ras exchange factor Son-of-sevenless. *J. Biol. Chem.* **270**, 15954–15957 (1995).
32. W. Wang *et al.*, The Grb2 binding domain of mSos1 is not required for downstream signal transduction. *Nat. Genet.* **10**, 294–300 (1995).
33. C. Zhao, G. Du, K. Skowronek, M. A. Frohman, D. Bar-Sagi, Phospholipase D2-generated phosphatidic acid couples EGFR stimulation to Ras activation by Sos. *Nat. Cell Biol.* **9**, 706–712 (2007).

34. L. B. Case, J. A. Ditlev, M. K. Rosen, Regulation of transmembrane signaling by phase separation. *Annu. Rev. Biophys.* **48**, 465–494 (2019).
35. A. S. Holehouse, R. V. Pappu, Functional implications of intracellular phase transitions. *Biochemistry*. **57**, 2415–2423 (2018).
36. J. C. D. Houtman *et al.*, Oligomerization of signaling complexes by the multipoint binding of GRB2 to both LAT and SOS1. *Nat. Struct. Mol. Biol.* **13**, 798–805 (2006).
37. R. L. Kortum *et al.*, The ability of Sos1 to oligomerize the adaptor protein LAT is separable from its guanine nucleotide exchange activity in vivo. *Sci. Signal.* **6**, ra99 (2013).
38. P. A. Boriack-Sjodin, S. M. Margarit, D. Bar-Sagi, J. Kuriyan, The structural basis of the activation of Ras by Sos. *Nature*. **394**, 337–343 (1998).
39. J. Cherfils, M. Zeghouf, Regulation of small GTPases by GEFs, GAPs, and GDIs. *Physiol. Rev.* **93**, 269–309 (2013).
40. K. Scheffzek *et al.*, The Ras-RasGAP complex: structural basis for GTPase activation and its loss in oncogenic Ras mutants. *Science*. **277**, 333–338 (1997).
41. K. Scheffzek, G. Shivalingaiah, Ras-Specific GTPase-Activating Proteins-Structures, Mechanisms, and Interactions. *Cold Spring Harb. Perspect. Med.* **9** (2019), doi:10.1101/cshperspect.a031500.
42. A. Hennig, R. Markwart, M. A. Esparza-Franco, G. Ladds, I. Rubio, Ras activation revisited: role of GEF and GAP systems. *Biol. Chem.* **396**, 831–848 (2015).
43. A. Aronheim *et al.*, Membrane targeting of the nucleotide exchange factor Sos is sufficient for activating the Ras signaling pathway. *Cell*. **78**, 949–961 (1994).
44. S. J. Leevers, H. F. Paterson, C. J. Marshall, Requirement for Ras in Raf activation is overcome by targeting Raf to the plasma membrane. *Nature*. **369**, 411–414 (1994).
45. D. K. Simanshu, D. V. Nissley, F. McCormick, RAS proteins and their regulators in human disease. *Cell*. **170**, 17–33 (2017).
46. Y. Zhou, P. Prakash, A. A. Gorfe, J. F. Hancock, Ras and the plasma membrane: A complicated relationship. *Cold Spring Harb. Perspect. Med.* **8** (2018), doi:10.1101/cshperspect.a031831.
47. W. Y. C. Huang *et al.*, A molecular assembly phase transition and kinetic proofreading modulate Ras activation by SOS. *Science*. **363**, 1098–1103 (2019).
48. M. T. Mazhab-Jafari *et al.*, Real-time NMR study of three small GTPases reveals that fluorescent 2'(3')-O-(N-methylanthraniloyl)-tagged nucleotides alter hydrolysis and exchange kinetics. *J. Biol. Chem.* **285**, 5132–5136 (2010).
49. S. M. Coyle, W. A. Lim, Mapping the functional versatility and fragility of Ras GTPase signaling circuits through in vitro network reconstitution. *Elife*. **5** (2016), doi:10.7554/eLife.12435.
50. S. J. Plowman, C. Muncke, R. G. Parton, J. F. Hancock, H-ras, K-ras, and inner plasma membrane raft proteins operate in nanoclusters with differential dependence on the actin cytoskeleton. *Proc. Natl. Acad. Sci. USA*. **102**, 15500–15505 (2005).

51. T. Gurry, O. Kahramanoğullari, R. G. Endres, Biophysical mechanism for ras-nanocluster formation and signaling in plasma membrane. *PLoS One*. **4**, e6148 (2009).
52. J. D. Rieker, J. C. Hu, Molecular applications of fusions to leucine zippers. *Meth. Enzymol.* **328**, 282–296 (2000).
53. P. Schuck, Use of surface plasmon resonance to probe the equilibrium and dynamic aspects of interactions between biological macromolecules. *Annu. Rev. Biophys. Biomol. Struct.* **26**, 541–566 (1997).
54. J. A. Zitzewitz, O. Bilsel, J. Luo, B. E. Jones, C. R. Matthews, Probing the folding mechanism of a leucine zipper peptide by stopped-flow circular dichroism spectroscopy. *Biochemistry*. **34**, 12812–12819 (1995).
55. L. Wiesmüller, A. Wittinghofer, Expression of the GTPase activating domain of the neurofibromatosis type 1 (NF1) gene in Escherichia coli and role of the conserved lysine residue. *J. Biol. Chem.* **267**, 10207–10210 (1992).
56. J. K. Chung *et al.*, K-Ras4B Remains Monomeric on Membranes over a Wide Range of Surface Densities and Lipid Compositions. *Biophys. J.* **114**, 137–145 (2018).
57. W. K. Gillette *et al.*, Farnesylated and methylated KRAS4b: high yield production of protein suitable for biophysical studies of prenylated protein-lipid interactions. *Sci. Rep.* **5**, 15916 (2015).
58. B. K. Jaitner *et al.*, Discrimination of amino acids mediating Ras binding from noninteracting residues affecting raf activation by double mutant analysis. *J. Biol. Chem.* **272**, 29927–29933 (1997).
59. J. T. Groves, N. Ulman, S. G. Boxer, Micropatterning fluid lipid bilayers on solid supports. *Science*. **275**, 651–653 (1997).
60. K. Scheffzek, A. Lautwein, W. Kabsch, M. R. Ahmadian, A. Wittinghofer, Crystal structure of the GTPase-activating domain of human p120GAP and implications for the interaction with Ras. *Nature*. **384**, 591–596 (1996).
61. M. R. Ahmadian, U. Hoffmann, R. S. Goody, A. Wittinghofer, Individual rate constants for the interaction of Ras proteins with GTPase-activating proteins determined by fluorescence spectroscopy. *Biochemistry*. **36**, 4535–4541 (1997).
62. M. J. Smith, B. G. Neel, M. Ikura, NMR-based functional profiling of RASopathies and oncogenic RAS mutations. *Proc. Natl. Acad. Sci. USA*. **110**, 4574–4579 (2013).
63. J. E. Scheffler *et al.*, Characterization of a 78-residue fragment of c-Raf-1 that comprises a minimal binding domain for the interaction with Ras-GTP. *J. Biol. Chem.* **269**, 22340–22346 (1994).
64. R. Gasper, F. Wittinghofer, The Ras switch in structural and historical perspective. *Biol. Chem.* **401**, 143–163 (2019).
65. A. Q. Khan *et al.*, RAS-mediated oncogenic signaling pathways in human malignancies. *Semin. Cancer Biol.* **54**, 1–13 (2019).
66. S. Boykevisch *et al.*, Regulation of ras signaling dynamics by Sos-mediated positive feedback. *Curr. Biol.* **16**, 2173–2179 (2006).

67. C. Lenzen, R. H. Cool, H. Prinz, J. Kuhlmann, A. Wittinghofer, Kinetic analysis by fluorescence of the interaction between Ras and the catalytic domain of the guanine nucleotide exchange factor Cdc25Mm. *Biochemistry*. **37**, 7420–7430 (1998).
68. C. Klebe, H. Prinz, A. Wittinghofer, R. S. Goody, The kinetic mechanism of Ran--nucleotide exchange catalyzed by RCC1. *Biochemistry*. **34**, 12543–12552 (1995).
69. L. E. Samelson, Signal transduction mediated by the T cell antigen receptor: the role of adapter proteins. *Annu. Rev. Immunol.* **20**, 371–394 (2002).
70. J. Schlessinger, Cell signaling by receptor tyrosine kinases. *Cell*. **103**, 211–225 (2000).
71. T. Shi *et al.*, Conservation of protein abundance patterns reveals the regulatory architecture of the EGFR-MAPK pathway. *Sci. Signal.* **9**, rs6 (2016).
72. A. Nag, M. I. Monine, J. R. Faeder, B. Goldstein, Aggregation of membrane proteins by cytosolic cross-linkers: theory and simulation of the LAT-Grb2-SOS1 system. *Biophys. J.* **96**, 2604–2623 (2009).
73. W. Y. C. Huang *et al.*, Phosphotyrosine-mediated LAT assembly on membranes drives kinetic bifurcation in recruitment dynamics of the Ras activator SOS. *Proc. Natl. Acad. Sci. USA*. **113**, 8218–8223 (2016).
74. X. Su *et al.*, Phase separation of signaling molecules promotes T cell receptor signal transduction. *Science*. **352**, 595–599 (2016).
75. W. Y. C. Huang, H.-K. Chiang, J. T. Groves, Dynamic Scaling Analysis of Molecular Motion within the LAT:Grb2:SOS Protein Network on Membranes. *Biophys. J.* **113**, 1807–1813 (2017).
76. W. Y. C. Huang, J. A. Ditlev, H.-K. Chiang, M. K. Rosen, J. T. Groves, Allosteric modulation of grb2 recruitment to the intrinsically disordered scaffold protein, LAT, by remote site phosphorylation. *J. Am. Chem. Soc.* **139**, 18009–18015 (2017).
77. B. J. Mayer, J. Yu, Protein clusters in phosphotyrosine signal transduction. *J. Mol. Biol.* **430**, 4547–4556 (2018).
78. S. Banjade, M. K. Rosen, Phase transitions of multivalent proteins can promote clustering of membrane receptors. *Elife*. **3** (2014), doi:10.7554/eLife.04123.
79. J. J. Hopfield, Kinetic proofreading: a new mechanism for reducing errors in biosynthetic processes requiring high specificity. *Proc. Natl. Acad. Sci. USA*. **71**, 4135–4139 (1974).
80. M. Tartaglia *et al.*, Gain-of-function SOS1 mutations cause a distinctive form of Noonan syndrome. *Nat. Genet.* **39**, 75–79 (2007).
81. J. C. D. Houtman *et al.*, Binding specificity of multiprotein signaling complexes is determined by both cooperative interactions and affinity preferences. *Biochemistry*. **43**, 4170–4178 (2004).
82. J. A. Nye, J. T. Groves, Kinetic control of histidine-tagged protein surface density on supported lipid bilayers. *Langmuir*. **24**, 4145–4149 (2008).
83. N. H. Shah *et al.*, An electrostatic selection mechanism controls sequential kinase signaling downstream of the T cell receptor. *Elife*. **5**, e20105 (2016).

84. W.-C. Lin *et al.*, H-Ras forms dimers on membrane surfaces via a protein-protein interface. *Proc. Natl. Acad. Sci. USA*. **111**, 2996–3001 (2014).
85. D. J. Williamson *et al.*, Pre-existing clusters of the adaptor Lat do not participate in early T cell signaling events. *Nat. Immunol.* **12**, 655–662 (2011).
86. K.-J. Cho, J. F. Hancock, Ras nanoclusters: a new drug target? *Small GTPases*. **4**, 57–60 (2013).
87. A. J. Stevens *et al.*, Design of a Split Intein with Exceptional Protein Splicing Activity. *J. Am. Chem. Soc.* **138**, 2162–2165 (2016).
88. C. B. McDonald *et al.*, Multivalent binding and facilitated diffusion account for the formation of the Grb2-Sos1 signaling complex in a cooperative manner. *Biochemistry*. **51**, 2122–2135 (2012).
89. J. R. Moffitt, Y. R. Chemla, C. Bustamante, in *Single Molecule Tools, Part B:Super-Resolution, Particle Tracking, Multiparameter, and Force Based Methods* (Elsevier, 2010), vol. 475 of *Methods in Enzymology*, pp. 221–257.
90. S. C. Kou, B. J. Cherayil, W. Min, B. P. English, X. S. Xie, Single-molecule Michaelis-Menten equations. *J. Phys. Chem. B*. **109**, 19068–19081 (2005).
91. J. Lin, A. Weiss, Identification of the minimal tyrosine residues required for linker for activation of T cell function. *J. Biol. Chem.* **276**, 29588–29595 (2001).
92. T. W. McKeithan, Kinetic proofreading in T-cell receptor signal transduction. *Proc. Natl. Acad. Sci. USA*. **92**, 5042–5046 (1995).
93. M. Turner, D. D. Billadeau, VAV proteins as signal integrators for multi-subunit immune-recognition receptors. *Nat. Rev. Immunol.* **2**, 476–486 (2002).
94. R. E. Cutler, R. M. Stephens, M. R. Saracino, D. K. Morrison, Autoregulation of the Raf-1 serine/threonine kinase. *Proc. Natl. Acad. Sci. USA*. **95**, 9214–9219 (1998).
95. B. P. Ziemba *et al.*, Single-molecule studies reveal a hidden key step in the activation mechanism of membrane-bound protein kinase C-α. *Biochemistry*. **53**, 1697–1713 (2014).
96. O. Vadas, J. E. Burke, X. Zhang, A. Berndt, R. L. Williams, Structural basis for activation and inhibition of class I phosphoinositide 3-kinases. *Sci. Signal.* **4**, re2 (2011).
97. L. B. Case, X. Zhang, J. A. Ditlev, M. K. Rosen, Stoichiometry controls activity of phase-separated clusters of actin signaling proteins. *Science*. **363**, 1093–1097 (2019).
98. Q. Yan *et al.*, Structural basis for activation of ZAP-70 by phosphorylation of the SH2-kinase linker. *Mol. Cell. Biol.* **33**, 2188–2201 (2013).
99. J. DelProposto, C. Y. Majmudar, J. L. Smith, W. C. Brown, Mocr: a novel fusion tag for enhancing solubility that is compatible with structural biology applications. *Protein Expr. Purif.* **63**, 40–49 (2009).
100. N. H. Shah, E. Eryilmaz, D. Cowburn, T. W. Muir, Extein residues play an intimate role in the rate-limiting step of protein trans-splicing. *J. Am. Chem. Soc.* **135**, 5839–5847 (2013).

BIBLIOGRAPHY

101. M. Tormen, E. Sovernigo, A. Pozzato, M. Pianigiani, M. Tormen, Sub-100μs nanoimprint lithography at wafer scale. *Microelectron. Eng.* **141**, 21–26 (2015).
102. A. D. Edelstein *et al.*, Advanced methods of microscope control using μManager software. *J. Biol. Methods*. **1** (2014), doi:10.14440/jbm.2014.36.
103. Kang Li @ CMU - Image Stabilizer Plugin for ImageJ, (available at http://www.cs.cmu.edu/~kangli/code/Image_Stabilizer.html).

Appendix A

Experimental Set-Up

A.1 Chemicals

Chapters 2 & 3

L-α-phosphatidylcholine (Egg, Chicken), Egg-PC; L-α-phosphatidylinositol-4,5-bisphosphate (Brain, Porcine), PIP2; 1,2-dioleoyl-sn-glycero-3-phosphoethanolamine-N-[4-(p-maleimidomethyl)cyclohexane-carboxamide], MCC-DOPE) (Avanti Polar Lipids, Alabaster, AL). The nucleotides used were: guanosine triphosphate (GTP), guanosine diphosphate (GDP), and guanosine 5′-[β,γ-imido]triphosphate (GppNHp) (Sigma-Aldrich, St. Louis, MO). Imaging buffer consisted of 10 mM β-mercaptoethanol (BME), 20 mM glucose, 2mM Trolox, 0.32 mg/mL glucose oxidase, 0.05 mg/mL catalase, and 0.02 mg/mL β-casein, all from Sigma-Aldrich except glucose oxidase (Serva Electrophoresis, Heidelberg, Germany).

Chapters 4

1,2-dioleoyl-sn-glycero-3-phosphocholine (DOPC) and 1,2-dioleoyl-sn-glycero-3- [(N-(5-amino-1-carboxypentyl) iminodiacetic acid) succinyl] (nickel salt) (Ni^{2+}-NTA- DOGS) were purchased from Avanti Polar Lipids. Texas Red 1,2-dihexadecanoylsn- glycero-3-phosphoethanolamine (TR-DHPE) was purchased from Invitrogen. Alexa Fluor 647 maleimide dye and Alexa Fluor 561 maleimide dye were purchased from Life Technology. Bovine Serum Albumin (BSA), (±)-6-Hydroxy-2,5,7,8- tetramethylchromane-2-carboxylic acid (Trolox), Catalase, 2-Mercaptoethanol (BME), $NiCl_2$, H_2SO_4 and ATP were purchased from Sigma-Aldrich. Glucose Oxidase was purchased from Serva. Tris(2-carboxyethyl) phosphine (TCEP) was brought from Thermo Scientific. Glucose and H_2O_2 were from Fisher Scientific. $MgCl_2$ was from EMD Chemicals. Tris buffer saline (TBS) was purchased from Corning.

A.2 Protein Purification

LAT and Grb2 Human LAT cytosolic domain (residues 30 to 233) and full-length Grb2 were purified as described previously(*98*) using an N-terminal 6-His tag. For Grb2, the N-terminal 6-His tag was removed with Tobacco Etch Virus protease.

H-Ras, SOS^{Cat}, NF1-333, p120-334. H-Ras (1-181, C118S) (human H-Ras protein with residues 1-181 and a point mutation to serine at residue C118 hereafter termed Ras), SOSCat Cys-lite (566-1049, C838A, C635A, C980S, and E718C), the GTPase activation (GAP) domain of NF1 (1198-1530) termed NF1-333, and the GAP domain of p120GAP (714-1047) termed GAP-334, were expressed and purified based on the protocols described in previous work(*13*, *22*). Briefly, plasmid was cloned into pET-20b vector, then transformed into Escherichia coli cells (Rosetta DE3) (Novagen, Darmstadt, Germany). Cells were lysed (50 mM Na2HPO4 (pH 8.0), 300 mM NaCl, 0.4 mM BME, 1 mM PMSF, and DNase) and recirculated over HiTrap (Co^{2+}) column. Protein was eluted with a linear gradient of 50 mM Na2HPO4 (pH 8.0), 300 mM NaCl, 0.4 mM BME, 500 mM imidazole and desalted overnight at 4 ˚C in 4 L of 50 mM Na2HPO4 (pH 8.0), 300 mM NaCl, and 0.4 mM BME with tobacco etch virus (TEV) protease (Sigma- Aldrich, St. Louis, MO) incubation. After a second HiTrap (Co^{2+}) column recirculation, protein was concentrated and gel-filtered using Superdex75 column in 20 mM Tris (pH 8.0, 200 mM NaCl, 5 mM MgCl2, 1 mM TCEP, 10 uM GDP). Appropriate fractions were pooled and concentrated to ~5 mg/mL then frozen for storage.

SOS^{HDPC}. SOS plasmid for SOS^{HDPC} (1-1049) was provided by J. Kuriyan, were expressed in Escherichia coli cells (BL21 DE3) (Novagen, Darmstadt, Germany). Cells were lysed in 25 mM Tris (pH 7.5), 500 mM NaCl, 0.4 mM BME, 1 mM PMSF, and DNase, and recirculated over HiTrap (Co^{2+}) column equilibrated in 25 mM Tris (pH 7.5), 500 mM NaCl, and 0.4 mM BME. Protein was eluted with a linear gradient of in 25 mM Tris (pH 7.5), 500 mM NaCl, 0.4 mM BME, and 500 mM imidazole before TEV protease treatment and dialysis in 4L of 25 mM Tris (pH 7.0), 300 mM NaCl, and 0.4 mM BME overnight at 4 oC. Cleaved His-tag was removed with HiTrap (Co2+) recirculation, and collected protein was concentrated in 25 mM Tris (pH 7.5), 50 mM NaCl, 1 mM TCEP and loaded onto MonoQ HP column. Protein was eluted with a linear gradient of 25 mM Tris (pH 7.5), 500 mM NaCl, 1 mM TCEP, concentrated, and gel-filtered using Superdex200 in 25 mM Tris (pH 7.5), 100 mM NaCl, 1 mM TCEP. 10% glycerol was added before further concentration and frozen before storage.

SOS^{CatPR} **.**Rosetta (DE3) bacteria were transformed with a T7 expression vector containing the ORF, His6-MBP-(Asn)10-TEV-SOSCatPR (533–1,333 aa; C838A, C635A, C980A) derived from the SOS1 human gene. Transformed bacteria were cultured in 10 L of Terrific broth media (22711-02; Invitrogen) at 37˚C. After OD600 reached .7, the temperature was lowered to 18˚C for one hour and expression was induced with 0.1 M isopropyl β-D-1-thiogalactopyranoside. Cells were allowed to grow for 10 hours at 25˚C and harvested by centrifugation. Cells were resuspended in 50 mM Na2HPO4 (pH=8), 500 mM NaCl, 0.4 mM BME, 1 mM PMSF, 20 µg/mL DNase, and 10% glycerol and lysed by microfluidization. The bacterial lysate was recirculated over two 5mL HiTrap chelating columns (GE Healthcare) charged with CoCl2. The HiTrap columns were extensively washed with 50 mM Na2HPO4 (pH=8), 500 mM NaCl, 0.4 mM BME before gradient elution with a buffer containing 50 mM Na2HPO4 (pH=8), 500 mM NaCl, 500mM Imidazole, 0.4 mM BME. Column eluate was dialyzed overnight into a buffer containing 50 mM Na2HPO4 (pH=8), 400 mM NaCl, and 0.4 mM BME in the presence of .1mg/mL TEV protease to cleave the His6-MBP-(Asn)10 tag.

After TEV site cleavage, Ser-Asn-Ala amino acids remain in the N-terminus of SOS^{CatPR}. After dialysis and tag cleavage, the protein was recirculated over a HiTrap chelating column where all his- tagged proteins are removed. The column flow-through, containing SOS^{CatPR}, was buffer exchanged into a buffer containing 20 mM Tris (pH=8), 50 mM NaCl, and 1 mM DTT and loaded into a MonoS cation exchange column (GE Healthcare) equilibrated with the same buffer. Bound SOS^{CatPR} (pI=8.57) eluted as a single peak between 120-275mM NaCl. Column eluate was spin concentrated with a Vivaspin 10 (GE Healthcare) and loaded into a Superdex200 (GE Healthcare) gel filtration column equilibrated in 20 mM Tris (pH 8), 200 mM NaCl, 10% glycerol, and 1 mM TCEP. Fractions with high purity of SOS^{CatPR} were collected and concentrated to 15 uM before freezing in liquid nitrogen and storing in -80˚C freezer.

SOS^{FL} .Expression and purification of full-length SOS protein (SOS^{FL}) from a bacterial expression system was unsuccessful as severe proteolysis would occur. In order to prevent proteolysis during the purification step, we used a split intein approach where we purified the N- and the C-terminal fragments of human SOS1 separately and to high purity. We then used the intein reaction to ligate the two fragments together(*87*) followed by another step of purification of the full-length protein.

The boundary between the N- and C-terminal fragments of SOS was placed in- between the CDC25 and PR domains, in a region that is predicted to be disordered. The amino-terminal SOS fragment (SOS^{N}; residues 2-1048) was cloned into a 2S-T vector containing an aminoterminal 6xHisSUMO tag (Addgene #29711). An amino-terminal consensus fast DnaE intein sequence (CfaN;(*87*)) followed by a monomeric Ocr fusion tag(*99*) was cloned following the carboxy-terminus of SOS-N. Mocr domain is highly acidic, and the addition of the domain helped the separation of SOSFL from unreacted SOS^{N} during the final purification on the MonoQ column (see below). The carboxy-terminal SOS fragment (SOS^{C}; residues 1049-1333) was cloned into a vector containing a hexahistidine tag followed by a TEV protease cleavage site and a NpuC intein sequence(*100*). The NpuC plasmid was a kind gift of Dr. Shah. Two mutations are added to the SOS^{C} sequence: T1049C introduced a catalytic cysteine residue for the intein reaction, and M1050F brought the preferable +2 residue for the efficient intein reaction(*87*).

Both fragments were overexpressed in Rosetta2(DE3) cells (Novagen). The transformed cells were grown at 37˚C in Terrific Broth media until OD600 reached 0.4. The protein expression was induced by addition of 0.5 mM IPTG at 18˚C for 14-18 hrs.

SOS^{N} expressing cells were suspended in Ni-N buffer (20 mM Tris pH 8.0, 1 M NaCl, 1 M Urea, 0.5 mM TCEP). The cells were lysed by sonication, and the insoluble fraction was separated by ultracentrifugation. The supernatant was applied to a HisTrap column (GE Healthcare), and SOS^{N} was eluted with 400 mM Imidazole. His6-SUMO tag was cleaved off by TEV protease while dialyzing against a Ni-N2 buffer (20 mM Tris pH 8.0, 500 mM NaCl, 500 mM urea, 5 mM β-mercaptoethanol) overnight. The cleaved SOS^{N} protein was reapplied to a HisTrap column and the flow-through was collected and concentrated on an Amicon Ultra

centrifugal filter unit (Millipore). Finally, the sample was purified on a S200 16/600 (GE Healthcare) size-exclusion column equilibrated with a SEC buffer (20 mM Tris pH 8.0, 300 mM NaCl, 0.5 mM TCEP). The pooled fractions were concentrated with an Amicon Ultra centrifugal filter unit, flash-frozen in liquid nitrogen and stored at -80˚C.

SOS^C expressing cells were suspended in Ni-C buffer (20 mM Tris pH 8.0, 500 mM NaCl, 500 mM urea, 0.5 % Triton, 0.5 mM TCEP) and purified on HisTrap in the same way as SOS^N. The eluate from the HisTrap column was dialyzed against a Ni-C2 buffer (20 mM sodium phosphate pH 6.5, 200 mM NaCl, 500 mM urea, 5 mM β- mercaptoethanol) while cleaving the tag with a TEV protease. The SOS^C fragment was then reapplied to the HisTrap column and separated from the uncleaved SOS^C fraction. The pooled fractions were diluted to half using a 20 mM sodium phosphate pH 6.5 buffer before applying to a HiTrap SP FF column (GE Healthcare) equilibrated with SP-A buffer (20 mM sodium phosphate pH 6.5, 100 mM NaCl, 500 mM urea, 1 mM DTT). A gradient of up to 1 M NaCl was applied and the fractions containing SOS-C were collected. The pooled fraction was flash-frozen by liquid nitrogen, and stored at -80˚C. The final yields of both SOS^N and the SOS^C fragments were about 2 mg per 1 L culture.

Purified SOS^N and SOS^C were mixed together at approximately 2 μM concentrations in an intein buffer (20 mM Tris pH 8.0, 100 mM NaCl, 5 mM TCEP) and incubated at 4˚C overnight. The ligated full-length SOS (SOS^{FL}) was diluted by 20 mM Tris pH 8.0 buffer to half the NaCl concentration and applied to a MonoQ column (GE Healthcare). The protein was purified on the column with MonoQ-A buffer (20 mM Tris pH 8.0, 50 mM NaCl, 0.5 mM TCEP) by applying a gradient of NaCl to 1 M. Typical yield of SOS^{FL} was about 30 %. The final SOS^{FL} protein contains two mutations: T1049C and M1050F, as a "scar" of the intein reaction, but otherwise the sequence is intact.

RBD-K65E . MGC human Raf-1 Sequence-Verified cDNA (Clone ID: 3904404), henceforth referred to as Raf1, was purchased from Dharmacon. The Ras-binding domain (RBD) of CRaf was PCR- amplified with Kpn1 and Not1 restriction sites flanking its N-terminus and C-terminus respectively. The sequence was cloned into a modified pETM-33 parent vector with an inserted SNAP-tag after the N-terminal his6-GST-3C site. A K65E point mutation of RBD was added using site-directed mutagenesis. BL21 (DE3) bacteria were transformed with a pETM11 expression vector containing the ORF, his6-GST-PreScission-SNAPtag-Raf1 RBD (56-131 aa; K65E) derived from the Raf-1 human gene. Transformed bacteria where cultured in 3 L of Terrific broth media (22711-02; Invitrogen) at 37˚C. After OD600 reached .8, the temperature was lowered to 18˚C for one hour and expression was induced with 0.1 M isopropyl β-D-1-thiogalactopyranoside. Cells were allowed to grow for 15 hours at 18˚C and harvested by centrifugation. Cells were resuspended in 50 mM Na2HPO4 (pH=8), 300 mM NaCl, 0.4 mM BME, 1 mM PMSF, and 20 μg/mL DNase and lysed by microfluidization. The bacterial lysate was recirculated over a 5mL HiTrap chelating columns (GE Healthcare) charged with $CoCl_2$. The HiTrap column was extensively washed with 50 mM Na2HPO4 (pH=8), 300 mM NaCl, 0.4 mM BME before gradient elution with a buffer containing 50 mM

Na2HPO4 (pH=8), 300 mM NaCl, 500mM Imidazole, 0.4 mM BME. The column eluate was dialyzed overnight into a buffer containing 50 mM Na2HPO4 (pH=8), 300 mM NaCl, and 0.4 mM BME in the presence of .1mg/mL PreScission protease to cleave the His6-GST tag. After dialysis and tag cleavage, the protein was recirculated over a HiTrap chelating column where all his- tagged proteins are removed. The column flow-through, containing SNAP-RBD, was spin concentrated with a Vivaspin 10 (GE Healthcare) and loaded into a Superdex75 (GE Healthcare) gel filtration column equilibrated in 20 mM Tris (pH=8), 200 mM NaCl, 10% glycerol, and .5 mM TCEP. RBD was concentrated to 87 uM before freezing in liquid nitrogen and storing in -80˚C freezer.

Same protocol was followed for the purification of SNAP-Leucine-Zipper-RBD, SNAP-RBD WT and SNAP-RBD (T68A).

Other RBD-Sensors .RBD, mCherry-RBD, RBD-mCherry, were purified following similar protocol, but using TEV protease for cleavage step.

A.3 Protein Labeling

Cysteine labeling

LAT, Grb2, SOS^{FL}, RBD (WT). Proteins were diluted to 100 μM (or less) with 5 mM TCEP. The proteins were then allowed to react with 1 mM Alexa Fluor 488, 555 or 647 maleimide dye for 2 hr in room temperature. The reaction was then quenched with 5 mM BME for 10 min. Excess dye was removed with multiple rounds of size exclusion chromatography (Sephadex G-25). For SOS^{FL}, excess dye was removed by dialysis overnight.

SOS^{HDPC}. SOS was labeled with Alexa Fluor 647 maleimide (Thermo Fisher Scientific, Waltham, MA) using a 1:2 reaction at room temperature. 100 mM BME was added 30 minutes after for an additional 10 minutes. Excess dye was removed using centrifugation filters and the labeled protein was gel filtered.

SNAP tag labeling

SNAP-RBD. Sensor was mixed with SNAP-Surface Alexa Fluor 488 (New England BioLabs, Ipswich, MA) at a 1:1.5 reaction in PBS and 10 mM DTT at 18˚C overnight. The solution was diluted in 20 mM Tris, 200 mM NaCl, 10% glycerol, and 1 mM TCEP before concentration and gel filtration.

A.4 Functionalized supported lipid bilayer

Chapter 2 & 3

Supported lipid bilayers (SLBs) functionalized with Ras were prepared based on methods described previously(*28*, *84*). Briefly, glass substrates were cleaned in 2% Hellmanex III solution (Hellma Analytics, Müllheim, Germany). They were sonicated in a 50:50 isopropanol (IPA): Milli-Q water (H2O) mixture and H2O for 15 minutes in each step. Glass substrates were etched in piranha solution (3:1 mixture of H_2SO_4: H_2O_2) for 5 minutes, rinsed with H2O, and adhered to sticky-Slide $VI^{0.4}$ open channel slides (Ibidi, Martinsried, Germany). A lipid mixture of 94% Egg-PC, 3% PIP2, and 3% MCC-DOPE in chloroform was rotorvapped and placed under nitrogen gas for 20 minutes. Dried lipid films were rehydrated in PBS to form a 1 mg/mL solution, which was extruded 15 times through a 30 nm pore-sized polycarbonate filter (EMD Millipore, Billerica, MA) to create small unilamellar vesicles (SUVs) before diluting to 0.5 mg/mL. SUVs were deposited in the assembled ibidi chambers and incubated for 30 minutes to form bilayers. 2 mg/mL β- casein and 0.4 mg/mL Ras diluted in PBS were added subsequently to the SLBs and incubated for 10 minutes and 2.5 hours respectively. Unreacted maleimide-modified lipid head groups were reduced after a 10 minute incubation in 5 mM BME. PBS buffer was exchanged to reaction buffer (40 mM HEPES, 100 mM NaCl, and 5 mM MgCl2, pH 7.4). Samples were stored overnight at 4˚C in 5 μM GDP diluted in reaction buffer, and were allowed to equilibrate to room temperature the next day before image acquisition.

Chapter 4

Chromium patterns (100 nm thick and 5 nm high) were fabricated by the Pulsed Nanoimprint Lithography method (Pulsed NIL)(*101*) (ThunderNIL Srl, Italy). Briefly, a stamp with desired patterns was fabricated by electron beam lithography, and was treated with hydrophobic trichlorosilanes to make it non-adhesive. Pulsed NIL was performed on glass substrates, which were previously spin coated with 120 nm thick mr-l 7010 resist, using the stamp. Residual resist film on the glass substrate was etched off using oxygen plasma before the chromium lift-off process. Nanopatterned substrates were cleaned with 2% Hallmanex III solution (Hellma Analytics) for 30 min followed by 15 min bath sonication in 1:1 IPA/H2O and H2O before piranha etching. Glass substrates (no. 1.5 thickness) were prepared by 5 min piranha etching (H2SO4:H2O2 = 3:1 by volume), followed by excessive rinsing of H2O (Milli-Q). Glass substrates were blow dried with air before depositing small unilamellar vesicles (SUVs) to form supported lipid bilayers (SLBs).

SUVs were prepared by mixing DOPC: Ni^{2+}-NTA-DOGS: PE MCC:PIP2 lipids = 92:4:2:2 by molar percent in chloroform. If visualization of the bilayers was required, an additional 0.005% of TR-DHPE were added to the lipid composition. The solution was then evaporated using a rotary evaporator for 15 min at 40°C. Dried lipid films were further blow dried with

N_2 for 15 min. Lipids were resuspended in H_2O by vortexing, resulting in a concentration of 1 mg/mL. Finally, the vesicle solution was sonicated for 90 s in an ice-water bath to make SUVs. The membrane reconstitution system was prepared on a flow chamber (μ-Slide, Ibidi). SLBs were formed on a glass substrate by incubating the SUVs mixed with 10 mM TBS for at least 30 min. The chambers were then rinsed with TBS buffer. TBS buffer refers to 20 mM TBS buffer with 5 mM $MgCl_2$ at pH 7.4 unless stated otherwise. Next, 1 mg/mL BSA in TBS buffer was incubated for 10 min to block defects in supported membranes. After rinsing, H-Ras was incubated at 0.4 mg/mL for 2 hr 30 min in TBS buffer. 5 mM BME was then added to stop the reaction. Next, the solution was buffer exchanged into TBS buffer containing 1 mM TCEP. Proteins were centrifuged for 20 min at 4°C beforehand to remove aggregates. Hck and LAT were incubated at 4 and 63 nM, respectively, for 10 min to attach to the bilayers via his-tag – Ni^{2+}-NTA chemistry (*82*). The system then sat for 20 min to let unstably bound membrane proteins to dissociate from the surface; during this step, 1 mM ATP and 100 μM GDP were included to phosphorylate LAT and ensure nucleotide loading in Ras. Between all incubation steps, the chambers were rinsed with TBS buffer. The fluidity of the membrane-bound proteins was examined by fluorescent recovery after photobleaching (FRAP) or single-particle tracking (SPT). Densities of membrane proteins were estimated by establishing a calibration curve between epifluorescence average intensity and densities measured by fluorescence correlation spectroscopy (FCS) (FCS methods were described previously(*84*)). All preparations were done at room temperature unless stated otherwise.

A.5 Optical Microscopy

Chapter 2 & 3

Images were acquired using total internal reflection fluorescence microscopy (TIRFM) on a Nikon Eclipse Ti inverted microscope with 100X oil immersion TIRF objective with 1.49 NA and an Andor iXon EMCCD camera. 488, 561, and 637 nm lasers from Coherent were used as illumination sources. The following filter sets were used for imaging: ET500LP and ET525/50M for 488 nm channel, ET575LP and ET600/50M for 561 nm channel, and ET660LP and 700/75M for 637 nm channel. The microscope was controlled using Micro-Manager(*102*) and aligned to produce Koehler illumination.

Chapter 4

TIRF experiments were performed on a motorized inverted microscope (Nikon Eclipse Ti-E; Technical Instruments, Burlingame, CA) equipped with a motorized Epi/TIRF illuminator, motorized Intensilight mercury lamp (Nikon C-HGFIE), Perfect Focus system, and a motorized stage (Applied Scientific Instrumentation MS-2000, Eugene, OR). A laser launch with 561 and 640 nm (Coherent OBIS, Santa Clara, CA) diode lasers was controlled by an OBIS Scientific Remote (Coherent Inc., Santa Clara, CA) and aligned into a fiber launch custom built by Solamere Technology Group, Inc. (Salt Lake City, UT). The optical path was then

aligned to a 100x 1.49 NA oil immersion TIRF objective (Nikon). A dichroic beamsplitter (ZT405/488/561/640rpc; Chroma Technology Corp., Bellows Falls, VT) reflected the laser light through the objective lens and fluorescence images were recorded using an EM-CCD (iXon 897DU; Andor Inc., South Windsor, CT) after passing through a laser-blocking filter (ZET405/488/561/640m-TRF; Chroma Technology Corp., Bellows Falls, VT). Laser powers measured at the sample were approximately 2.7 mW and 0.7 mW for 561 nm and 647 nm, respectively. Exposure times were set to 40 ms and 20 ms for 561 nm and 647 nm, respectively. All acquisitions were obtained using Micro-Manager(*102*). A TTL signal from the appropriate laser triggered the camera exposure

A.6 Ras Density Calibration

Chapter 2 & 3

RBD sensor intensity conversion to Ras-GTP level was calibrated using Ras-functionalized SLBs prepared on glass slides with Ras concentrations between 0.05 and 0.6 mg/mL. After BME incubation, Ras was loaded with 5 μM GppNp-Atto488 using 20 nM SOS^{Cat} in reaction buffer to catalyze nucleotide exchange for a minimum of 10 minutes. Samples were washed with 1 mL of 10 mM BME in reaction buffer immediately before fluorescence correlation spectroscopy (FCS) measurements. Samples were washed with 2 mL reaction buffer and bound nucleotide was exchanged to unlabeled GTP in a 10-minute incubation with 1 mM GTP and 20 nM SOS^{Cat} Cys-Lite. Background fluorescence was measured using TIRFM after samples were rinsed with 2 mL reaction buffer. Images were acquired 5 minutes after injection of 50 nM of RBD sensor in IB. Intensities of all images per sample were averaged after subtraction of background fluorescence and plotted against the measured Ras density to produce the calibration curve displayed below:

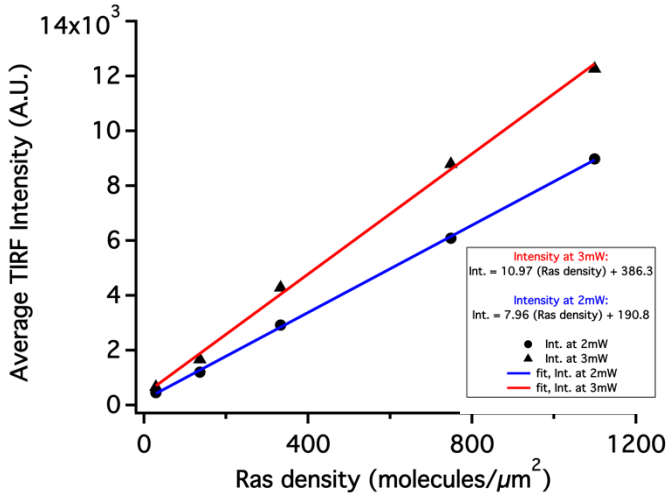

A.7 Ras activation microarray assay with single SOS imaging

Chapter 3

Ras-tethered SLBs prepared the previous day was equilibrated to room temperature. In experiments that evaluated effects of Ras-GTP on SOS catalytic activity, an additional nucleotide exchange step was performed. These samples were washed with 2 mL of stripping buffer (40 mM HEPES and 150 mM NaCl) and incubated in 50mM EDTA, 40 mM HEPES, 150 mM NaCl for 20 minutes. They were washed with another 2 mL of stripping buffer before addition of 100 uM of GDP or GTP in reaction buffer. All samples were washed with 2 mL of reaction buffer before imaging.

Images were acquired before and 5 minutes after the addition of 50 nM RBD sensor in IB into the sample to measure background fluorescence and starting Ras-GTP density. 50 nM RBD sensor, 1 mM GTP, and SOS^{HDPC} or SOS^{FL} between 1 nM and 50 nM in IB was added at the beginning of time-lapse acquisition. In conditions where deactivation pressure from GAPs were tested, 500 pM of NF1-333 was added concurrently with SOS. Alexa488-RBD sensor was imaged every 10 or 20 s, and SOS^{HDPC}-Alexa647 or SOS^{FL}-Alexa555 was imaged simultaneously every 1 to 10 s for 30 to 60 minutes. The total Ras density in each corral was measured at the end of the time-lapse after a 5-minute incubation of 20 nM SOS^{Cat} and 1 mM GTP in reaction buffer and addition of 50 nM RBD sensor in IB to fully activate all Ras molecules.

Chapter 4

All imaging experiments were performed in imaging buffer consisted of 2 mM UV-treated trolox, 10 mM βME, 20 mM glucose, 320 μg/mL glucose oxidase, 50 μg/mL catalase (52) and 0.01 mg/mL Casein in TBS buffer. To trigger SOS recruitment, ~1 nM SOS^{FL}-Alexa Fluor 555, 20 nM Grb2, 10 nM RBD-K65E-Alexa Fluor 647, and 120 μM GTP were added into solution with the imaging buffer. This set of conditions will result mostly in either one or zero SOS recruited per corral during a 10-min imaging session. We performed the corral assay at a very dilute SOS^{FL} concentration (~ 1 nM), such that at any given time, only about ~ 3% of the corrals were occupied with a SOS molecule (accounting for its labeling efficiency). Therefore, the probability of two SOS molecules localized to the same corral at a given time is < 0.1% (estimated with Poisson statistics).

In our experiments, spectral bleed-through is minimal since both 561 and 647 dyes are on proteins with very low densities (unlike conventional bulk colocalization experiments). SOS channel is strictly at the single-molecule level (averaged density < 0.05 μm^{-2}); initial accumulation of RBD (at the timescale that activation time of SOS is measured) has very little detectable signals in the 561 channel.

Time-lapse acquisition was taken at a framerate of 0.5 Hz with a very low power (~2.7 mW for 561 before the objection). This acquisition strategy allows long visualization (> 100 s) of SOS localization by lowering the photobleaching rates (bleaching time was ~130 sec with imaging buffers); bleaching rate was estimated from immobilized SOS on glass substrates.

The analysis was performed on the central square of 300×300 pixel to decrease uneven illumination. Further processing corrected the remaining uneven illumination in the region of interest: the time-lapse images were background-subtracted and field illumination corrected in Fiji; Stage drift was corrected using the 'Image Stabilizer' FIJI plugin(*103*). Intensity profiles for individual corrals were extracted and further analyzed with a custom script in MATLAB 2016.

Image processing. Background intensity subtraction and field illumination correction were performed on the TIRFM images using ImageJ. Custom code on MATLAB was used to identify the chromium grid that segments the SLB and to generate coordinates of each corralled region. Fluorescence intensities of the regions at each time point were extracted using MATLAB and converted to number of Ras activated. Reaction trajectories were analyzed in custom made code in MATLAB.

Statistics A typical set of experiments (on a single day) involves 6-12 independent supported membrane microarray chips, each of which have ≥ 2,000 experimentally resolvable membrane corrals. From the ~2,000 corrals imaged in each experiment, ~ 200 single-molecule observations/trajectories were collected with the remaining ~1800 corrals providing robust background measurement as well as providing controls for spatial variation in the sample or other sources of error. This collected data was used to construct the histograms (Fig. 4.2, 4.3). Then, the full set of experiments were repeated independently on a different day for a minimum of 3 additional iterations; experiments with the PR domains (Fig. 4.4) were repeated 3 times. To benchmark the assay between different days, we repeated the condition of Grb2-mediated full-length SOS activation as a standard (≥ 10 fully independent iterations).

Appendix B

Data Analysis

B.1 Data Analysis Chapter 3

Kinetic rate equations

In the absence of GEFs, the rate at which Ras-GTP density $\boldsymbol{x_{Ras.GTP}}$increases due to passive exchange of bound GDP to GTP from solution is described as:

$$\frac{\mathrm{d}x_{Ras.GTP}}{dt} = k_i x_{Ras.GDP}$$

Where $\boldsymbol{x_{Ras.GDP}}$ represents Ras-GDP density, $k_i$is the intrinsic nucleotide exchange rate constant, and $\boldsymbol{t}$ is time. Upon addition of SOS at concentration **[SOS]**, the rate of Ras-GTP production in traces with no burst in Ras activation is:

$$\frac{\mathrm{d}x_{Ras.GTP}}{dt} = \left(k_i + k_{eff}[\mathrm{SOS}]\right)x_{Ras.GDP}$$

Where $\boldsymbol{k_{eff}}$ represents the effective catalytic rate constant of SOS in the transient state. In the scenario where a single SOS molecule in the processive state is stably recruited to the membrane, the rate of Ras activation is:

$$\frac{\mathrm{d}x_{Ras.GTP}}{dt} = \left(k_i + k_{eff}[\mathrm{SOS}] + k'\right)x_{Ras.GDP}$$

Where $\boldsymbol{k'}$ is the rate at which a single SOS turns over Ras molecules.

Effective catalytic rate constant analysis. Ras-GTP values measured 10 min after SOS addition allowed clear differentiation between corrals that experienced burst activation from those that did not at or before this selected time point. The distribution of Ras-GTP numbers at 10 min. Ras activation traces from corrals with Ras-GTP level below the mean plus two times the standard deviation ($\boldsymbol{\mu + 2\sigma}$) with no identified change points at 10 min were plotted. These traces were then used to compute the effective catalytic rate constant (**keff**) of SOS using the equation presented on **Fig 3.3B**.

Calculation of the probability of SOS to enter processive state. Corrals were determined to experience bursts in Ras activation if two or more change points in the intensity traces were identified. Ras-GTP level was segmented into 100 molecule intervals, and the number of Ras-GTP at the onset of each burst activation was determined (**Fig. 3.4A**, red dots). Histograms of burst activation events that occur in each interval was summed and plotted as a function of Ras-GTP for both SOS^{HDPC} and SOSFL. These distributions were normalized by the cumulative time (τ) spent by all corrals at each Ras-GTP interval (Fig. 3.4 B,C). The resulting distributions yield the probability of the two SOS constructs to transition to the processive state relative to Ras-GTP number using the equation:

$$\mathrm{P}(\text{ processive SOS observed in Ras. GTP} = [\mathrm{x}, \mathrm{x}+\Delta)\ ) = \frac{\#\ burst\ events\ in\ [\mathrm{x},\mathrm{x}+\Delta)}{\tau\ [\mathrm{x},\mathrm{x}+\Delta)}$$

Where **Δ** is 100 and **x** is an arbitrary Ras-GTP value.

B.2 Data Analysis Chapter 4

Activation time analysis. Trajectory analyses were performed with MATLAB 2016, after preprocessing from Fiji. The intensities of SOS and RBD channels were plotted after smoothing with average filtering of 5 and 7 data points, respectively. The change points of each channel were analyzed with the "findchangepts" function in MATLAB. For SOS channel, a change point was detected when the mean changed; for RBD channel, a change point was detected when the slope (i.e. rate of Ras-dGTP production) changed. The threshold used depends on the mean and noise of the intensities. The performance of the thresholds used was benchmarked with corrals without SOS recruitment (Fig. S3D) and corrals with SOS activation (Fig. 1D). In our application, we found a threshold of 12,000 and 20,000 worked well for strict change-point detection of SOS and RBD, respectively. The activation time **X** for each trajectory was then evaluated as such:

$$t_{act} = \tau_{Ras.GTP} - \tau_{SOS}$$

if the RBD channel has a change point while SOS is recruited Eq. [S1]

where t_i denotes the time of the first change point. For the rejection time t_{rej}, it is calculated as:

$$t_{act} = \tau'_{SOS} - \tau_{SOS}$$

if the RBD channel has no change point before SOS dissociates Eq. [S2]

where τ' denotes the second change point, or dissociation from membranes. The rejection time is the dwell times of SOS given that no activation occurs. Corrals without recruited SOS

were discarded from the analysis. In some rare trajectories, a corral can have two SOS on membranes (roughly doubling the intensities) at the same time; these trajectories were also filtered from the analysis. A representative analysis of interpretable SOS and RBD trajectories are shown in Fig. 4.1D, E.

Spontaneous activation of SOS. SOS is primarily shuttled onto membranes by Grb2. In the absence of Grb2, SOS can, in rare cases, temporarily escape from autoinhibition and recruit to membranes through binding Ras at its allosteric pocket. This receptor-independent activation is characterized to have an exponential activation time distribution (Fig. 4.3). This activation pathway contributes, though minorly (~10%), to SOS activation even under the presence of Grb2. To quantify the activation time distribution for Grb2-mediated pathway, we subtracted the estimated receptor- independent contribution from the activation time histogram of SOS^{FL} activation with Grb2. Receptor-independent activation contributes less in the case of SOS^{CatPR} activation since the lack of N-terminal autoinhibition causes Grb2-mediated recruitment of SOS^{CatPR} to increase by 3-fold compared to SOS^{FL}; therefore, we did not subtract the receptor- independent count in this case.

Goodness-of-fit analysis for Fig. 3. The following table shows the reduced chi- squared analysis of Fig. 4.3F-I between $N = 1$ intermediate and exponential kinetics ($N = 0$). The model (Fig. 4.3A-D) is supported with lower reduced chi-squared statistics, although only marginally in the case without PIP2. Therefore, we further analyze the goodness-of-fit for the proofreading ratio, p_{rej}/p_{act}, for the case without PIP2. Comparing the prediction of model with the data, the residual sum of squares for $N = 0$ and $N = 1$ are 1.03 ×103 and 5.83 ×102, respectively. Therefore, $N = 1$ describes the case without PIP2 better over $N = 0$.

Model	SOS^{FL}	*w/o Grb2*	SOS^{catPR}	*w/o* PIP_2
$N = 0$	8.6×10^{-7}	9.1×10^{-7}	2.1×10^{-7}	1.304×10^{-7}
$N = 1$	2.5×10^{-7}	10.2×10^{-7}	5.2×10^{-7}	1.298×10^{-7}

Dwell time analysis. Single molecules were tracked with a customized program written in Igor(*73*). The analysis was performed on the central 350×350 pixel region of the images to minimize uneven illumination. The dwell times from each binding event were sorted into a histogram with the frame interval as the bin. The histogram was normalized and fitted to a probability distribution of multi-exponential kinetics:

$$p(t) = \sum_{i=1}^{N} \alpha_i k_i e^{-k_i t} \qquad \text{Eq. [S3]}$$

where N is the number of population, α_i is the fraction of the population I and ki is the rate constant for the population i. A typical histogram consisted of 2,000-5,000 data points. Fitting procedure initiated with a single exponential. In cases of poor fitting, a maximum of two populations was used.

APPENDIX B. Data Analysis

Step-size distribution analysis. Single-molecule were tracked with a customized program written in Igor(*73*). The analysis was performed on the central 350×350 pixel region of the images to minimize uneven illumination. The step size between each frame was sorted into a histogram with a bin of 0.02 μm. The histogram was normalized and fitted to a probability distribution of a single or double freely diffusive population:

$$p(t) = \sum_{i=1}^{N} \alpha_i \frac{r}{2D_i\Delta t} e^{-\frac{r^2}{4D_i\Delta t}} \quad \text{Eq. [S4]}$$

where N is the number of population, α_i is the fraction of the population I and Di is the diffusion coefficient for the population i. Immobilized particles were filtered from the analysis.

Activation kinetics of SOS. In the following, we derive the activation time and rejection time distribution for a simple model of SOS activation(*73*). For a cytosolic enzyme to activate on membrane surfaces at time t, it must satisfy two conditions: ***i***) the enzyme reaches the activation state at time t, and ***ii***) the enzyme remains bound to the membrane. This molecular description leads to a probabilistic statement of the activation time distribution $p_{act}(t)$:

$$p_{act}(t) = p_N(t)P(t < T_D) = p_N(t) \cdot e^{-k_{-1}t} \quad \text{Eq. [S5]}$$

where t is the time, T_D is the random variable for the time to dissociate from membranes, $p_N(t)$ is the distribution of the activation kinetics, and P denotes the cumulative probability. The dissociation of a molecule from membranes is assumed to be a Poisson process with a rate constant k_{-1}. Considering the simplifying case where the individual kinetic intermediates have equal rate constants, $p_N(t) = k_N^{N+1} t^N e^{-k_N t}/N!$, where N is the number of kinetic intermediates each with a transition rate constant k_N. This simplification is particularly a good approximation where the intermediate(s) are well-resolved in the experimental timescale. For the rejection time distribution, $p_{rec}(t)$ can be expressed in a similar argument:

$$p_{rec}(t) = P(t < T_N)p_D(t) = \int_t^\infty p_N(t')dt' \cdot k_{-1}e^{-k_{-1}t} = \frac{\Gamma(N,t)}{N!} \cdot k_{-1}e^{-k_{-1}t} \quad \text{Eq. [S6]}$$

where T_N is the random variable for the time to activate on membranes, $p_D(t)$ is the distribution of dissociation, and, $\Gamma(N,t) = \int_{k_N t}^\infty t'^N e^{-t'} dt'$, which is the upper incomplete gamma function. Note that in our definition, the probability of activation, $P_{act}(t)$, can be easily obtained by $P_{act}(t) = \int_t^\infty p_{act}(t)dt$; a similar expression also defines the probability of rejection, $P_{rej}(t) = \int_t^\infty p_{rej}(t)dt$;, such that $P_{act} + P_{rej} = 1$.

Fig. 4.4 parameter definition The fold-increase of SOS activity is defined as $x_{SOS} = \frac{P_{act,activated} - P_{act,basal}}{P_{act,basal}}$, where the probability of activation is calculated following the previous equations. The basal state refers to the unassembled, monovalent SOS interaction with LAT via Grb2.